

# Nature of laminations and mineralization in rhinoceros enamel using histology and X-ray synchrotron microtomography: Potential implications for palaeoenvironmental isotopic studies

Paul Tafforeau<sup>a,b,c,\*</sup>, Ilhem Bentaleb<sup>a</sup>, Jean-Jacques Jaeger<sup>a,c</sup>, Céline Martin<sup>a</sup>

<sup>a</sup> *Institut des Sciences de l'Evolution, UMR CNRS 5554, cc 064, Université de Montpellier II, pl. E. Bataillon, 34095 Montpellier cedex 05, France*

<sup>b</sup> *European Synchrotron Radiation Facility, 6 rue Horowitz BP 220, 38046 Grenoble Cedex, France*

<sup>c</sup> *Laboratoire de Géobiologie, Paléogéographie et Paléontologie Humaine, UMR CNRS 6046, Université de Poitiers, 40 Avenue du Recteur Pineau, 86022 Poitiers cedex, France*

Received 30 November 2005; received in revised form 25 August 2006; accepted 3 October 2006

## Abstract

Incremental features of rhinoceros molar enamel were studied quantitatively on histological slices. The different kinds of incremental features of enamel were related to one another and counted to determine the rate and duration of crown formation and to clarify the status of the laminations. The mineralization and the microstructure of the enamel were examined in a rhinoceros molar germ using X-ray synchrotron microtomography respectively using absorption and phase contrast mode at different levels of resolution, from 45.71  $\mu\text{m}$  for the largest scale up to 0.28  $\mu\text{m}$  for the finest one. The different microtomographic data were combined to obtain a multiscale integrated overview of the microstructure and mineralization in order to understand better the relationship between these two aspects. Additional human and herbivorous mammal teeth were examined qualitatively using histological sectioning to obtain a better understanding of laminations in mammal tooth enamel.

Laminations, regularly spaced features parallel to the Retzius lines, represent regular isochrons of enamel deposition. This study shows that laminations and cross-striations are equivalent daily features in enamel of rhinoceros, humans, and probably of middle sized and large herbivorous mammals in general. Laminations are shown to be three-dimensional alignments of cross-striations. In addition to the fact that cross-striations are visible only in prismatic enamel, observation of histological slices, and high resolution phase contrast X-ray synchrotron microtomography demonstrate three main parameters influencing the dominant aspect of daily features in rhinoceros and human enamel: the angle between prisms and Retzius lines, the enamel deposition rate and the thickness of the histological slices. Given their daily nature, laminations can be used to determine the crown formation time of middle sized and big herbivorous mammals.

Quantitative study of the enamel mineralization in the rhinoceros germ fragment using X-ray synchrotron microtomography suggests that the innermost 20  $\mu\text{m}$  of the enamel near the enamel–dentin junction are highly mineralised (77–90% of the final enamel mineralization) during, or just after the deposition of the corresponding enamel matrix. Integrated microtomographic study shows that this area corresponds to the thin aprismatic enamel layer at the EDJ level plus a thin layer of radial enamel directly adjacent. It appears that, in some parts of the enamel, there may be a considerable time lag between matrix deposition and full maturation, which could have important implications for geochemical studies. This study reinforces the previously suggested hypothesis that isotopic measurements derived from the innermost enamel may represent the period most closely related to matrix

\* Corresponding author. European Synchrotron Radiation Facility, 6 rue Horowitz BP 220, 38046 Grenoble Cedex, France. Tel.: +33 438 88 19 74; fax: +33 476 88 22 52.

E-mail address: [paul.tafforeau@esrf.fr](mailto:paul.tafforeau@esrf.fr) (P. Tafforeau).

secretion. By using information derived from incremental features (laminations and Retzius lines) and restricting the isotopic measurements to the innermost part of the enamel, precise temporal calibration of isotopic signals should be possible, and the complication of time averaging due to enamel maturation could be avoided or strongly reduced.

© 2006 Elsevier B.V. All rights reserved.

*Keywords:* Enamel incremental features; Crown formation time; Enamel – dentin junction; Enamel maturation; X-ray synchrotron microtomography; Laminations; Palaeoenvironment

## 1. Introduction

### 1.1. Enamel formation and estimation of crown formation time

The formation of mammal dental enamel is a complex process that is still not fully understood. It can be divided into two principal phases (Suga, 1983). The first one is the secretion by the ameloblasts of the enamel matrix (Reith and Butcher, 1967) (partially mineralized organic web which serves to guide the final mineralization of the enamel). The second one is the maturation of this matrix (Allan, 1967; Reith and Butcher, 1967; Suga, 1983), which consists of the progressive removal of the organic matrix and of the increase in enamel mineralization that leads to a final hydroxyapatite concentration of about 95% in weight (Sakae et al., 1997; Passey and Cerling, 2002). This extremely high mineralization of the enamel explains the fact that teeth compose the major part of the mammal fossil record. Enamel is generally well preserved during fossilization, and is subjected to relatively few modifications (Fearnhead, 1984; Koenigswald, 1997).

In addition to numerous palaeobiological studies on fossil teeth, another aspect of dental enamel has been highlighted over the last few years. As this tissue grows incrementally (Moss-Salentijn et al., 1997; Fitzgerald, 1998; Shellis, 1998) and undergoes no modification during the entire life of the animal, it can be used as a proxy for palaeoenvironmental studies by measurement of the stable isotopes of oxygen and carbon (Longinelli, 1984; Bryant et al., 1996; Iacumin et al., 1996). Some isotopic studies on enamel consisted of analyses of bulk samples that furnished general data about average palaeoenvironmental parameters [see for example (Ayliffe et al., 1992; Bryant et al., 1994; Zazzo et al., 2002)]. Recently, high temporal resolution studies were carried out in order to quantify seasonal palaeoclimatic variations (Fox and Fisher, 2001; Balasse et al., 2002; Zazzo et al., 2002; Macho et al., 2003; Hoppe et al., 2004a). However, these studies encountered more or less the same problems: the establishment of a precise time scale independent of the

isotopic measurements, and minimization of the time averaging in each sample. These problems are directly linked to the different aspects of the enamel formation in its two phases. Maturation of the enamel is not synchronized with matrix deposition, and the topology of the maturation front is not necessarily similar to the one of the matrix secretion front (Balasse, 2003): these two fronts do not necessarily progress at the same rate (Allan, 1967; Passey and Cerling, 2002; Hoppe et al., 2004b). Sampling and calculating time by using incremental features in the enamel could lead to erroneous interpretations of the isotopic record. The method used to perform the sampling can also greatly influence the results (Zazzo et al., 2005).

For a given location, mineralization following matrix secretion may be delayed, and it can take weeks to months from the beginning of the maturation process to the fully mineralized enamel (Hoppe et al., 2004b), which causes a major problem for high-resolution isotopic studies (Passey and Cerling, 2002; Passey et al., 2005; Zazzo et al., 2005). In fact, a single sample, even taken at a very precise point, does not represent an instantaneous measurement but an average over a longer time period.

Previous studies on enamel maturation have shown that in several groups, including primates, artiodactyls, rodents and carnivores, the innermost enamel layer adjacent to the enamel–dentin junction (EDJ) is strongly mineralized just after its formation (Allan, 1967; Suga, 1983, 1989). This zone is also subjected to the maturation process, but the increase in mineralization is far much less than in the other parts of the enamel. As previously suggested (Balasse, 2003) and recently experimentally investigated, with a low sampling resolution (Zazzo et al., 2005), isotopic measurements performed on this inner zone could lead to data mainly synchronous with the matrix deposit, i.e. with the incremental features. In this study we used X-ray synchrotron microtomography (Tafforeau, 2004; Tafforeau et al., 2006) to assess if this zone of high initial mineralization exists in rhinoceros enamel, and if so, to determine its thickness and quantitative mineralization with a very high resolution. This method is a powerful

tool to investigate mineralization patterns on bones or teeth with a high resolution (Nuzzo et al., 2002; Tafforeau, 2004; Dowker et al., 2004, 2006).

Despite the fact that enamel development has been studied extensively for primates and some other mammals with brachydont teeth, very few data are available for large herbivorous mammals. Recently, some studies proposed estimations of mineralization time of the enamel for some large herbivorous mammals (Gadbury et al., 2000; Hoppe et al., 2004b), but they were based on radiographic observations on modern animals. It is extremely difficult to observe early dental germs on radiographs (because the early mineralization of the enamel matrix is not detected), and to determine precisely the exact time of the final crown completion (Beynon et al., 1998). Thus, radiographs tend to underestimate the formation time of a tooth, and cannot be directly related to data obtained by studies on incremental marks in enamel. Additionally, although this technique may yield information about enamel maturation for living mammals, it cannot be applied to fossils because of remineralization of unerupted dental germs during fossilisation process.

Histological techniques based on counts and measurements of incremental features in enamel currently constitute the only way to determine crown formation time (CFT) in fossil teeth, although these techniques do not yield data on enamel maturation. Information derived from incremental marks may precisely represent matrix secretion rate and duration, but without consideration of the subsequent mineralization, the actual total time of formation (i.e. matrix deposition plus maturation) is underestimated. These techniques have been widely applied to primates (Dean et al., 1993; Reid et al., 1998a,b; Dirks et al., 2002; Dean and Schrenk, 2003; Schwartz et al., 2003; Smith et al., 2003, 2004), but very few data are available for middle sized and large herbivorous mammals (Macho et al., 2003).

The aims of this study were threefold: 1) to assess if the method of CFT determination in primate enamel could be applied to or adapted for rhinoceros teeth; 2) to clarify whether the laminations observed are daily features and to elucidate their relationship with cross-striations; and 3), to examine the mineralization pattern at the enamel–dentin junction in rhinoceros teeth using very high precision methods. These histological and microtomographic observations were used then to propose strategies for isotopic studies, in order to obtain high resolution results from fossil enamel with minimized time averaging due to delayed maturation.

## 1.2. Incremental marks in enamel

We first determined whether the findings of numerous studies of primate enamel could be applied to studies of enamel development in herbivorous mammals. We worked in particular on rhinoceros, in order to develop a method for measuring CFT on modern and large fossil teeth. We chose rhinoceros as a model group because they are very well represented in the fossil record and can present different dental morphologies, from nearly bunodont to hypsodont teeth.

Ameloblasts undergo cyclic variations during their secretory activity that lead to the formation of incremental features in the matrix, which still remain visible in mature enamel (Boyde et al., 1988). Among these features, the cross-striations reflect the circadian variations of ameloblast activity. This last point has been clearly demonstrated by Bromage (1991) and Smith (2004, 2006). In primate teeth they appear as short straight lines perpendicular to the prisms (Gustavson and Gustavson, 1967).

The Retzius lines are a second kind of incremental features. They are accentuated lines that correspond to successive positions of the ameloblast front at regular periods (Gustavson and Gustavson, 1967; Risnes, 1990, 1998). They reflect a long-period cycle in the ameloblast activity. In the imbricational (lateral or non-cuspal) part of the enamel, Retzius lines reach the outer surface of the tooth and correspond to external regular rings known as perikymata. The time between the formation of two consecutive Retzius lines, i.e. of a Retzius band, is called periodicity. It can be determined by counting the number of prism cross-striations per Retzius band. The periodicity varies for different species and can even vary for different individuals of the same species, but it is constant for all teeth of a single individual (Fitzgerald, 1998; Schwartz et al., 2001; Smith et al., 2003). The periodicity in primate teeth is 2–12 d (Dean, 1987; Ramirez-Rozzi, 1993; Fitzgerald, 1998; Risnes, 1998; Schwartz et al., 2001; Dean and Schrenk, 2003; Kelley and Smith, 2003; Schwartz et al., 2003; Smith et al., 2003).

Once the periodicity of Retzius lines is known, counting the total number of Retzius bands on an adequate vertical slice in an unworn tooth gives a good estimation of the duration of the imbricational CFT. Estimation of the cuspal time of primate teeth requires other methods (Risnes, 1986; Dean, 1998), as Retzius lines are often poorly visible in the cuspal part of the enamel.

A third kind of incremental mark has been observed in primate enamel: the laminations. As these features are

regularly spaced and parallel to Retzius lines, they should also represent regular isochrons of enamel deposition. Their status among mammals still remains unclear. Observations with scanning electron microscopy on etched primate enamel (Risnes, 1998) tend to show that they are directly linked to cross-striation. Previous studies on fossil primate teeth argued that laminations do not appear to be daily (Smith et al., 2003, 2004). However, in a recent study using fluorescent marking on macaque teeth, Smith revised her position and showed clearly the daily nature of the laminations (Smith, 2004, 2006) and their temporal equivalence with cross-striations. By studying rhinoceros enamel, we aim to verify if laminations reflect circadian rhythms in other mammals, as do cross-striations. Given their predominance in rhinoceros enamel and other herbivorous mammals, if laminations are equal to cross-striations, they could be

used for quantitative developmental studies of middle sized and large herbivorous mammal teeth, which could be used to calibrate isotopic palaeoenvironmental studies.

## 2. Material and methods

### 2.1. Study Samples

For this study, we used fossil rhinoceros teeth of *Rhinoceros sondaicus*, cf. *Gaindatherium*, *Diaceratherium aurelianense* and *Brachypotherium stehlini*. We also studied modern rhinoceros teeth of *Rhinoceros unicornis* and *R. sondaicus*.

We used a third upper molar ( $M^3$ ) from a complete fossil skeleton of *Rhinoceros sondaicus*, discovered in a pit in Kalasin Province NE Thailand ( $16^{\circ}30' N$ ,  $104^{\circ}15' E$ , Fig. 1A). Attempts of radiocarbon analysis on both

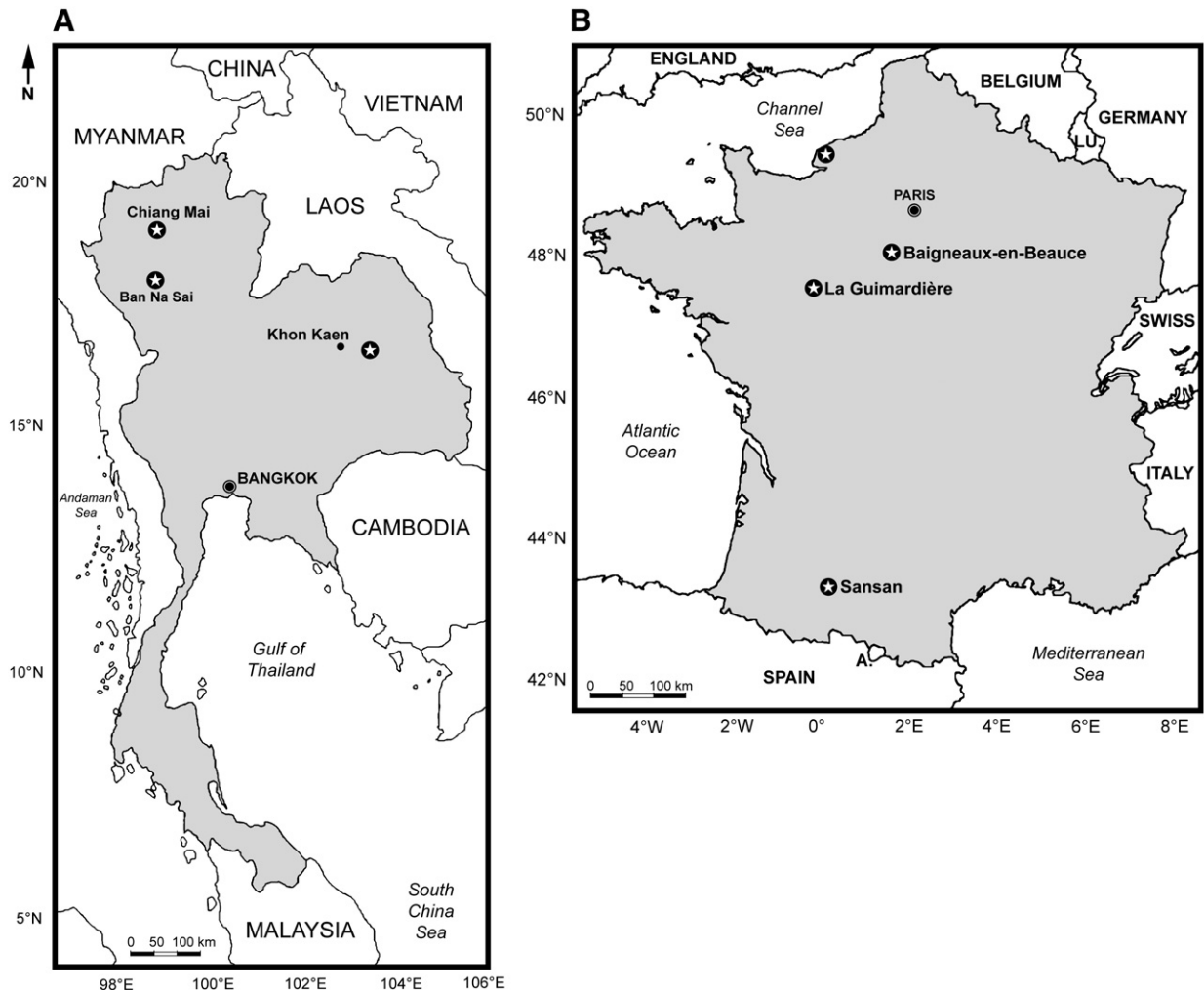


Fig. 1. Maps of Thailand (A) and France (B) showing the provenance of the different samples used in this study.

the enamel of M<sup>3</sup> (in Kiel, Germany) and associated bone fragments (in Gif-sur-Yvette, France) failed due to low tooth carbon content and porous bone fragments. Low uranium content made U–Th dating on bones of the same specimen (35–88 ka) inaccurate. The attempt gave an age of 57 ka (+31/–22)(±1σ); Based on biostratigraphy we attribute an Upper Pleistocene age to the *R. sondaicus* skeleton.

A third lower molar (M<sub>3</sub>) attributed to a fossil rhinoceros cf. *Gaindatherium* (closely related to the extant *R. sondaicus*) was recovered from a Middle Miocene lignite in a sub-basin at Ban Na Sai in NW Thailand (18°3' N, 100°5' E, Fig. 1A) in Li basin. The few distinct mammals (suids, anthracotheriids, rhinocerotids, and stegolophodon mastodons) from the Ban Na Sai locality are believed to be related to genera from well-dated localities in China, Pakistan and India (Siwaliks), leading to a late Middle Miocene age assignment (Ducrocq et al., 1995). This is confirmed by magnetostratigraphic data showing that the main period of sedimentation of these Northern Thai intramontane basins occurred between 14 and 12 Ma (Benammi et al., 2002; Chaimanee et al., 2003).

A first upper molar (M<sup>1</sup>) was extracted from the skull of a modern juvenile individual of *Rhinoceros unicornis* from the zoological park of Chiang Mai in Thailand (18°48'22.4" N, 98°56'48.9" E, Fig. 1A). This tooth is used as an extant reference sample.

The distal part of the ectoloph of an upper molar of *Diaceratherium aurelianense* was recovered in the Lower Burdigalian (20.5–19.5 Ma) site of La Guimardière (47°32' N, 0°1' E, Maine-et-Loire, France, Fig. 1B). Two teeth fragments of *Brachypotherium stehlini* (the mesial part of the ectoloph of a right upper molar, and the protoconid of a right lower molar) from the Upper Burdigalian (17–17.5 Ma) site of Baigneaux-en-Beauce (48°07' N, 01°49' E, Eure-et-Loir, France, Fig. 1B) were also studied.

Three teeth were used for the quantitative histological study of the incremental features: the M<sub>3</sub> of cf. *Gaindatherium*, the M<sup>3</sup> of *Rhinoceros sondaicus* and the M<sup>1</sup> of *Rhinoceros unicornis*. No counting was performed on the two teeth of *Brachypotherium stehlini*, and that of *Diaceratherium aurelianense*. The incremental marks were observed only for qualitative purposes, in order to understand the general organisation of the different growth features of several species of rhinoceros.

To study quantitatively the enamel mineralization, we used two fragments of an early third upper molar germ of a modern *Rhinoceros sondaicus* from Laos. A part of the *R. unicornis* M<sup>1</sup> it was also used to measure

the mineral density of mature rhinoceros enamel using X-ray synchrotron microtomography.

In order to obtain a more general qualitative characterization of incremental features, we prepared some teeth of large herbivorous mammals: modern cows (*Bos taurus*) and horses (*Equus caballus*) from Seine-Maritime (49°44' N, 0°38' E, France, Fig. 1B), and an enamel fragment of a fossil *Elephantidae* from the Middle Miocene site of Sansan (43°32' N, 0°35' E, Gers, France, Fig. 1B). Some human teeth were also prepared to compare the incremental features between a primate (*Homo sapiens sapiens*), and rhinoceros.

## 2.2. Sample preparation and analysis of incremental features

For analyses of growth features, teeth were embedded in polyester resin. They were vertically sectioned through the highest cusp using a 0.35 mm thick diamond saw, to prepare sections of 1 mm thickness. The cuts, glued on a microscope glass slice with Araldite epoxy resin CY 230, were ground to a thickness of 100 μm using silicon carbide of decreasing size. At this stage, the thin sections were polished with aluminum oxide (0.05 μm), and then covered with a cover slip glued with the same epoxy resin. The samples were observed in natural and polarized light using an optical microscope (Leitz Ortholux II) coupled with a digital camera (Olympus DP12). Using Adobe® Photoshop® software, we reconstituted the entire enamel area of each vertical slice at a 25×-magnification (mosaic images) to draw and count the Retzius lines. We used higher magnification (100×) in about ten areas to observe finer incremental marks. For each of these areas, we made mosaic pictures of the entire thickness of the enamel.

At 25×-magnification, Retzius lines were clearest in the outer part of the enamel (Fig. 2A), but they could be easily followed and traced all along their course. Defining the Retzius lines with overlays permitted their course to be illustrated (Fig. 2B), and distinguished from laminations at the EDJ. Retzius lines in the imbricational part of the enamel were confirmed by the observation of perikymata directly on the teeth or on their casts (Fig. 2C). For the cuspal enamel, as the Retzius lines do not reach the enamel surface, it is impossible to observe perikymata. Nevertheless, by comparison with the imbricational enamel and by precise observation of the laminations and of some quite visible cuspal Retzius lines, it is possible to distinguish Retzius lines from laminations in the cuspal part of the enamel. Composite images, consisting of superimposition of the 25× and

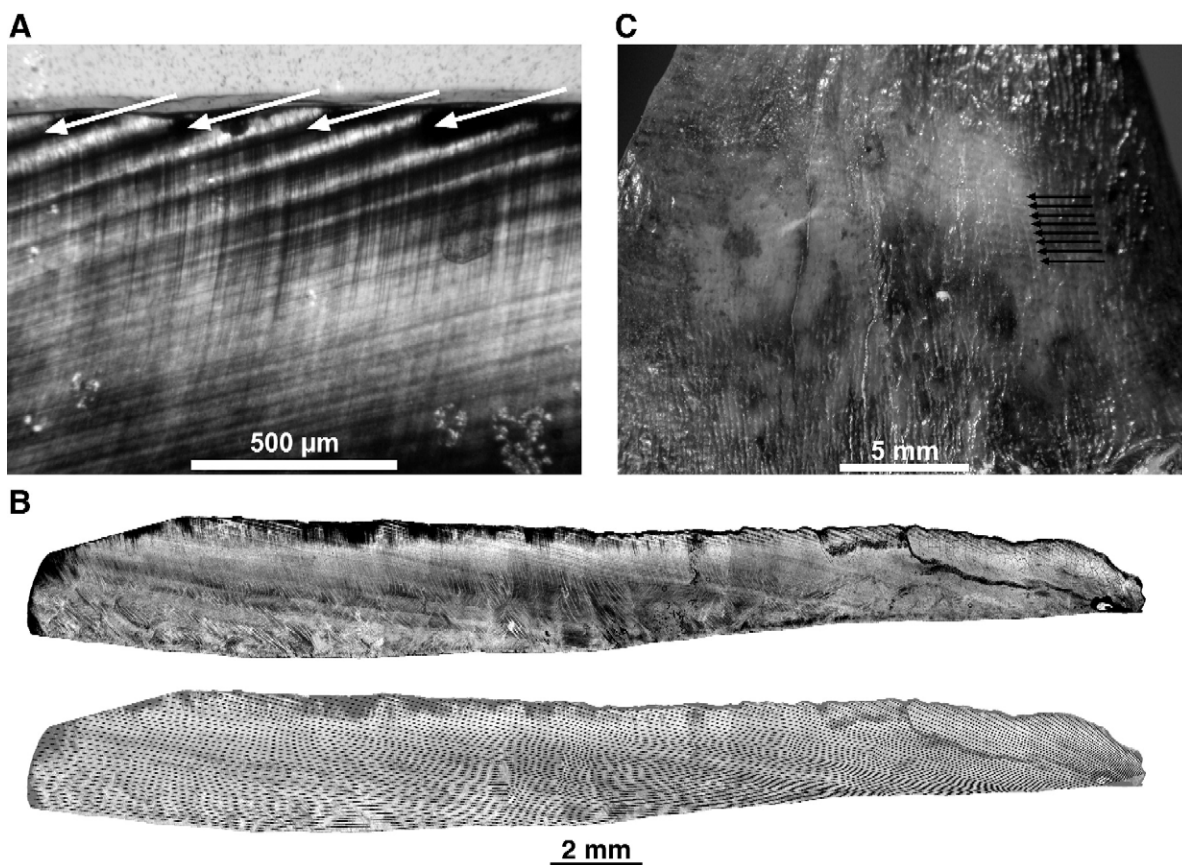


Fig. 2. A: Retzius lines in transmitted light microscopy in the outer imbricational enamel of the cf. *Gaioadatherium* M<sub>3</sub>. B: Comparison of overview and overlay showing Retzius lines from the outer enamel to the enamel–dentin junction (EDJ) on the M<sub>3</sub> of cf. *Gaioadatherium*. The EDJ is on the bottom and the occlusal face of the tooth is to the left. C: Perikymata on an upper molar fragment of *Diaceratherium aurelianense* (external view).

100× magnification pictures, permitted Retzius lines overlays and the laminations to be imaged together. This method may introduce some uncertainty in the counting of the laminations per Retzius band due to the limited precision of the Retzius lines overlaying. Hence, numerous counts in different areas of the tooth were made in order to statistically estimate the periodicity of the Retzius lines using laminations.

### 2.3. Analysis of mineralization pattern of the enamel–dentin junction

For the study of the enamel mineralization, we performed several microtomographic scans on two fragments of the modern *Rhinoceros sondaicus* M<sup>3</sup> germ, and on a part of the *R. unicornis* M<sup>1</sup>. We used X-ray synchrotron microtomography at the European Synchrotron Radiation Facility (ESRF, Grenoble, France) on the beamlines ID17 and ID19 (Salvo et al.,

2003; Tafforeau, 2004; Feist et al., 2005; Tafforeau et al., 2006). All three-dimensional reconstructions were performed using the VGStudio Max 1.2 software (Volume Graphics). The technical parameters of the different scans are presented in Table 1.

For the quantitative determination of enamel mineralization, we used the protocol proposed by Nuzzo et al. (2002) to calculate the mineral density of the enamel using the measured linear absorption coefficients in our sample. We considered mass attenuation coefficients of hydroxyapatite ( $MAC_{HA}$ ) to be  $0.988 \text{ cm}^2/\text{g}$  at 40 keV,  $1.389 \text{ cm}^2/\text{g}$  at 35 keV and  $3.482 \text{ cm}^2/\text{g}$  at 25 keV (Nuzzo et al., 2002). We used those values as calibration references for the calculation of the mineral content of the enamel assuming that it is composed only of hydroxyapatite (HA). Since the germ was dried, we considered enamel on that sample as a monophasic system with only HA and air. As we used a monochromatic beam, the mineral density ( $d_{HA}$ )

Table 1  
Technical parameters of the different X-ray synchrotron microtomographic scans

Sample	Beamline	Voxel size (μm)	Energy (keV)	Monochromator	Propagation distance (mm)	Imaging Mode	Angular step (degrees)	Field of view (mm)	Number of scans
<i>R. sondaicus</i> M <sup>3</sup> germ	ID17	45.71	60	Double Si cristal	5000	Absorption	0.12	96	1
<i>R. unicornis</i> M <sup>1</sup>	ID19	32.12	40	Double Si cristal	40	Absorption	0.3	16.5	5
<i>R. sondaicus</i> M <sup>3</sup> germ	ID19	10.12	35	Double Si cristal	40	Absorption	0.18	20	2
<i>R. sondaicus</i> M <sup>3</sup> germ	ID19	5.06	35	Double Si cristal	990	Phase contrast	0.12	10.3	2
<i>R. sondaicus</i> M <sup>3</sup> germ	ID19	1.4	25	Multilayer	4	Absorption	0.15	1.4	5
<i>R. sondaicus</i> M <sup>3</sup> germ	ID19	0.7	25	Multilayer	25	Phase contrast	0.12	1.4	1
<i>R. sondaicus</i> M <sup>3</sup> germ	ID19	0.28	19	Multilayer	10	Holotomography	0.12	0.6	1

expressed in grams of HA per cm<sup>3</sup> was directly obtained from the measured linear attenuation coefficient ( $\mu$ ) on the microtomographic slices using the equation:

$$d_{\text{HA}} = \mu / MAC_{\text{HA}}$$

For the investigations of the incremental features on the *R. sondaicus* germ, we used two phase contrast imaging techniques: propagation phase contrast and holotomography.

Propagation phase contrast requires increasing the distance between the camera and the sample. Due to the high coherence of the X-ray beam at the ID19 beamline of the ESRF, increasing the sample/detector

distance reveals an interference pattern of the X-ray beam generated by the different interfaces in the sample (Buffière et al., 1999; Cloetens et al., 1999a,b; Baruchel et al., 2000, 2001; Salvo et al., 2003; Tafforeau et al., 2006). This technique permitted observation of the Retzius lines on the larger fragment of the germ with a 5.06 μm voxel size, and revealed the enamel microstructure and fine incremental features on a scan using a voxel size of 0.7 μm. Nevertheless, in order to clearly resolve the 3D organization of the fine incremental features, we performed a phase contrast scan with a voxel size of 0.28 μm that was processed as holotomographic scan. Holotomography was originally developed for pure

Table 2  
Results of incremental marks counts and estimations of enamel deposit duration

	cf. <i>Gaiotherium</i> M <sub>3</sub> (slice 1)	cf. <i>Gaiotherium</i> M <sub>3</sub> (slice 2)	<i>Rhinoceros unicornis</i> M <sup>1</sup>	<i>Rhinoceros sondaicus</i> M <sup>3</sup>
Number of Retzius bands	98±5	95±5	92±10	152±10
Number of Retzius bands showing laminations	43	70	67	51
Number of counts of laminations	119	106	178	98
Mode of laminations per Retzius band (periodicity)	7	7	7	7
Average of laminations per Retzius bands	7.02	6.88	6.85	6.76
Standard deviation	0.91	0.66	0.66	1.11
$\tau$	0.212	-0.046	-0.006	0.252
$Z\tau$	3.41	-0.70	-0.12	3.68
$p$	0.0006 <sup>a</sup>	0.4867	0.902	0.0002 <sup>a</sup>
Recorded time (days)	686±35	665±35	644±70	1064±70
Extrapolated missing Retzius bands	Slice 1: 17±5 (Fig. 5A)		Nearly unworn tooth	28±10 (Fig. 5B)
Estimated CFT (days)	Slice 1: 805±70		644±70	1260±140
Estimated CFT (years)	Slice 1: 2.2±0.2		1.8±0.2	3.5±0.4

<sup>a</sup> Kendall  $\tau$  test showing significant variations of the amount of laminations per Retzius Bands during the enamel matrix deposit.

phase objects (without absorption) and theoretically requires several scans taken at several distances in order to obtain all the frequencies in the projections after the phase retrieval process (Cloetens et al., 1999a, b). We used a Gaussian blur filtering of each of the original projections in order to remove the large scale absorption and obtain a virtually pure phase object. The phase retrieval algorithm was then used on that single scan assuming that the missing frequencies were not in the range of the structures we aimed to enhance. This resulted in reconstructed slices with a far better visibility of the enamel prisms and fine incremental lines than with the original phase contrast scan. These data were used to investigate the 3D organisation of cross-striations and their relation with laminations, and also to determine the enamel microstructure of the highly mineralized area at the level of the EDJ.

Another aspect is particularly interesting when using microtomographic data: performing an averaging of several successive slices is equivalent to a virtual slice with anisotropic voxel size, the slice thickness corresponding exactly to the number of averaged slices. This technique permits to generate projection slices in the direction of specific structures and then to increase the contrast of these structures present on all the slices relatively to all the other non-constant structures without defocusing effect. This technique could be compared to projections generated using optical slices produced by a confocal microscope.

### 3. Results

#### 3.1. Histological study of incremental features and crown formation time

The Retzius lines were clear on all rhinoceros samples observed at low magnification (50×). Using 200 times magnification, growth lines parallel to these Retzius lines (Fig. 3A) can be observed that seem to be equivalent to those that are described as laminations for primate enamel (Risnes, 1998; Smith et al., 2003; Smith, 2004, 2006). However, the incremental features comparable to those observed in rhinoceros enamel have been described as cross-striations in primate enamel (Bromage, 1991), and recently in horse cheek teeth (Hoppe et al., 2004b).

We examined the number and distribution of Retzius lines and laminations in three rhinoceros teeth, in order to quantitatively check the duration of their formation and to verify whether laminations are suitable for developmental and palaeoenvironmental studies. The results are summarized in Table 2.

The counts on different slices of the three teeth showed Gaussian distributions with a mode of seven laminations per Retzius band (Fig. 3B). We suggest that random fluctuations of the counting is due to the imprecision of the Retzius lines overlays on the low-resolution pictures. A Gaussian distribution was less clear for the *Rhinoceros sondaicus* M<sup>3</sup>. Kendall  $\tau$  test on the periodicity related to the successive Retzius bands from the cervix of the tooth towards the cusps tips showed no significant variation for two slices out of four. On the two slides that showed significant variation laminations were relatively difficult to observe, which may explain the results of the tests for these two slices. Despite this finding, we believe

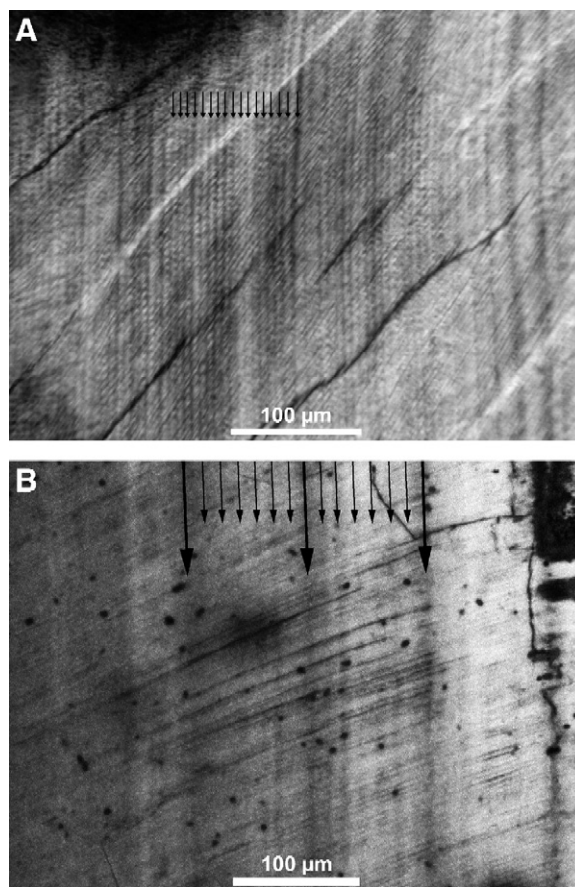


Fig. 3. A: Transmitted light microscopy of the laminations (labelled with black arrows) in an upper molar fragment of *Diaceratherium aurelianense*. B: Simultaneous observation of laminations and Retzius lines on the outer enamel of the M<sub>3</sub> of cf. *Gaioadatherium* imaged with a confocal microscope (Biorad 1024 CLSM system mounted on a Nikon Optiphot II upright microscope and an Argon-Krypton ion laser). Seven laminations (demarcated by small arrows) can be seen between two successive Retzius lines (big arrows).

that the periodicity remains constant during enamel deposition.

Fig. 4A and B present the distributions of the Retzius lines respectively along the EDJ and the external surface. We used the cervix as reference for comparisons since some of our samples presented significant wear. Despite a time reversal relative to the actual developmental path (zero correspond to the completion of the matrix deposit instead of the

initiation of the cusp), such a representation allows quantitative comparisons of the crown extension rates (Fig. 4A) and of the perikymata distribution (Fig. 4B) on the lateral enamel without effect of the wear. It also allows a comparison of these parameters even if the total CFT of these teeth are very different. In Fig. 4A it is possible to see that the crown extension rates of the lateral enamel are very similar for the two M3 (cf. *Gaioadatherium* M<sub>3</sub> and *R. sondaicus* M<sup>3</sup>) for the last 600 days of their formation. Extension rates of the lateral enamel are also very similar for all the studied teeth for the last 300 days of their formation with an average EDJ extension rate of 11.5  $\mu\text{m}/\text{d}$ . During the first half of its development, the crown extension rate of the M<sup>1</sup> of *R. unicornis* is clearly higher than those of the two M3 with a maximum extension rate reaching 47.6  $\mu\text{m}/\text{days}$  on the cusp tip. In the Fig. 4B, the two M3 also show quite similar distribution of perikymata, but due to the strong wear of the cf. *Gaioadatherium* molar, this comparison can be done only for the last 460 days of the matrix formation, corresponding to a length of 21.5 mm along the external surface. In contrast, the M<sup>1</sup> presents a very different pattern for the perikymata distribution corresponding to relatively lower angles of the Retzius lines at the EDJ related to the faster development of that tooth compared to the two M3.

In order to estimate the CFT of the two worn teeth (the cf. *Gaioadatherium* M<sub>3</sub> and the *R. sondaicus* M<sup>3</sup>), we estimated the missing cuspal enamel using profiles from unworn teeth (Fig. 5), and extrapolated the course of missing Retzius lines from the pattern of those present by using the extension rates graphs presented in the Fig. 4A.

As no data are available for the timing of dental eruptions of *Rhinoceros unicornis*, we suggest that the age of the first upper molar eruption for this species may well be quite similar to that observed for the other rhinoceros taxon, *Ceratotherium simum*, which is between 1.5 to 3 years (Hillman-Smith et al., 1986). In this case, a CFT of less than two years for this *R. unicornis* M<sup>1</sup> corresponds to what may be expected. We interpreted an accentuated incremental line observed on this tooth in both enamel and dentin (Fig. 6) as the neonatal line commonly observed in primates (Gustavson and Gustavson, 1967; Risnes, 1998) which is believed to be caused by the stress experienced during and just after birth. We counted 37 Retzius bands formed intra-utero on this M<sup>1</sup>. Given a seven-day periodicity of Retzius lines calculated on the basis of laminations, this tooth began to develop about 9 months before the birth of this individual and the

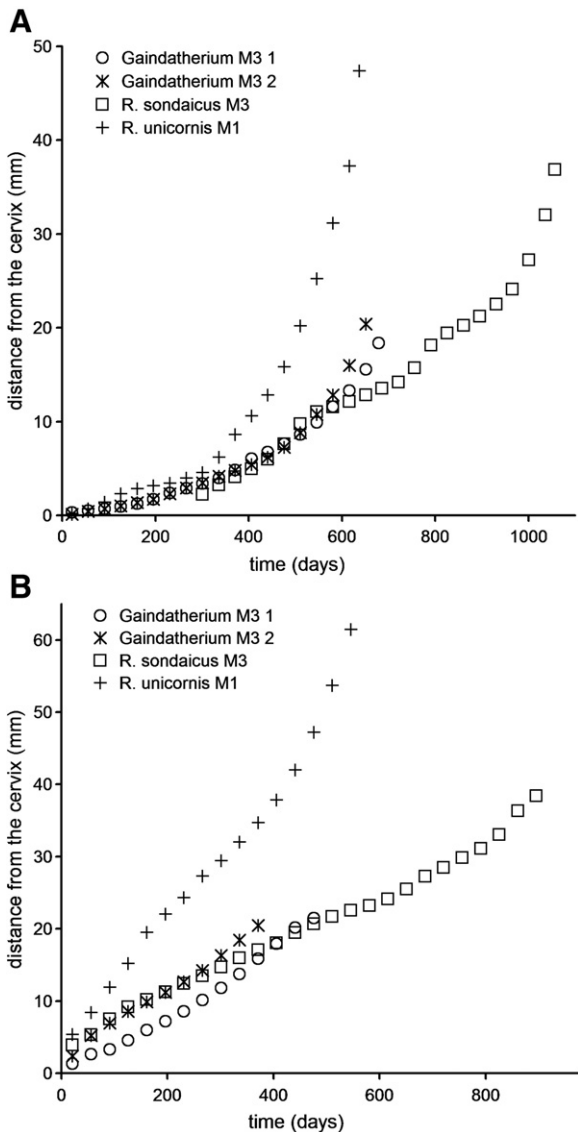


Fig. 4. Distribution of the Retzius lines along the EDJ and the external surface from cervix to apex in function of time (expressed in days assuming a seven-day periodicity of Retzius lines for all the samples). A: Position of Retzius lines along the EDJ, corresponding to crown extension rates. B: Position of Retzius lines along the external surface corresponding to the distribution of perikymata.

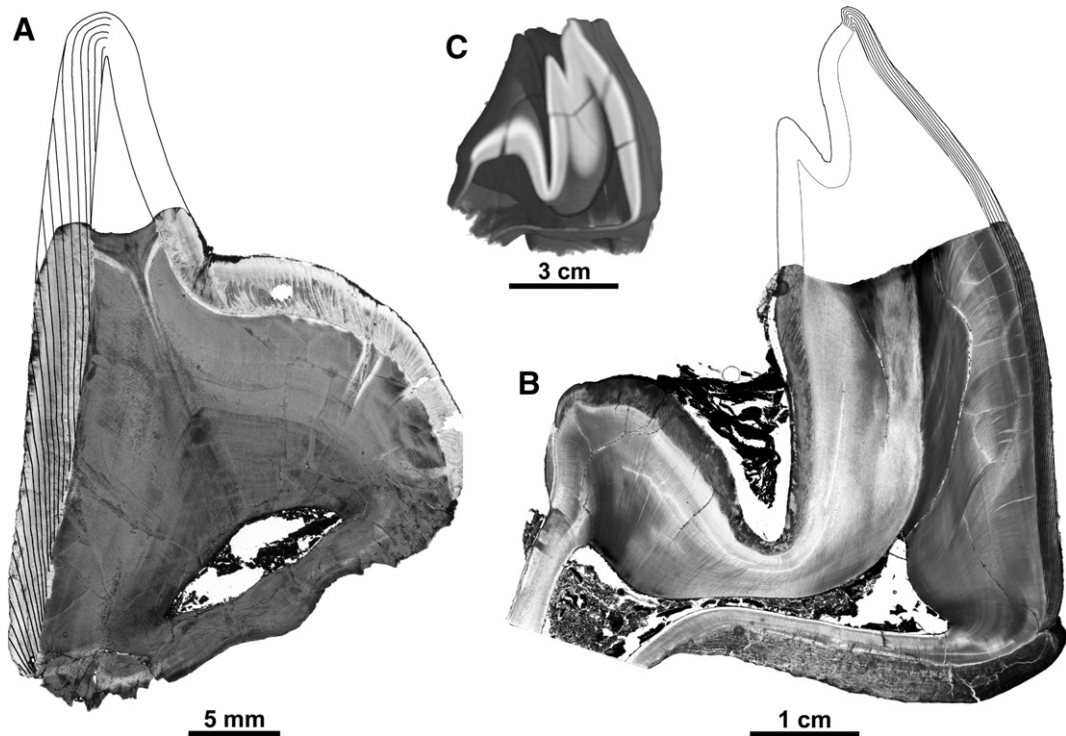


Fig. 5. A: Reconstruction of the worn part of the cf. *Gaidatherium* M<sub>3</sub>. The external form of the missing enamel was reconstructed from a cut in a cast of an unworn lower molar of *Rhinoceros unicornis*. The EDJ was extrapolated from the observed enamel thickness on the unworn part of the slice. B: Reconstruction of the worn part of the *Rhinoceros sondaicus* M<sub>3</sub>. The missing enamel was reconstructed on the basis of an equivalent virtual cut through an unworn molar of *Dicerorhinus sumatrensis* (C) imaged with a medical scanner (scanner LightSpeed 16, 120 kV, 100 mA, pixel size 150  $\mu$ m, slice thickness 450  $\mu$ m). For both A and B, the orientation and spacing of missing Retzius lines were extrapolated from the continuation of those observed on the unworn enamel, and by an estimation at the level of the EDJ of their putative initial spacing. Only one line out of five was drawn for clarity.

matrix was completely formed about 13 months after birth. The gestation time of this species is estimated to about 16 months (Owen-Smith, 1995). Consequently,

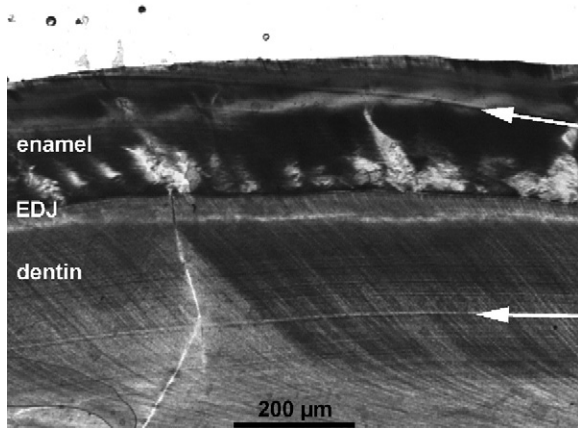


Fig. 6. Strongly accentuated line in the enamel (top white arrow) of the M<sup>1</sup> of *Rhinoceros unicornis* interpreted to be the neonatal line, which is also clear in the dentin (bottom white arrow).

our histological results are compatible with biological observations on both gestation length and first molar emergence times.

Qualitative observations of three samples of *Brachypotherium stehlini* and *Diaceratherium aurelianense* using 250 times magnifications (Fig. 7) show laminations that are not straight lines but are, in fact, alignments of small incremental features similar to primate cross-striations. Along a single prism, these features can show distances of about 10  $\mu$ m ( $9 \pm 0.2$   $\mu$ m,  $N=117$  for *B. stehlini* and  $10.8 \pm 0.2$   $\mu$ m,  $N=93$  for *D. aurelianense*) in contrast to an average of about 4  $\mu$ m in the cuspal enamel of several hominoid primates (Dean, 1998). The measurements of distances were taken along single prisms on series of five successive laminations in the middle part of the imbricational enamel. Considering the respective sizes of human and of rhinoceros third molars, and that both kinds of teeth take about three years to form, (Reid et al., 1998b), it suggests that the rhinoceros enamel apposition rate is about 2.5 times faster than that of humans.

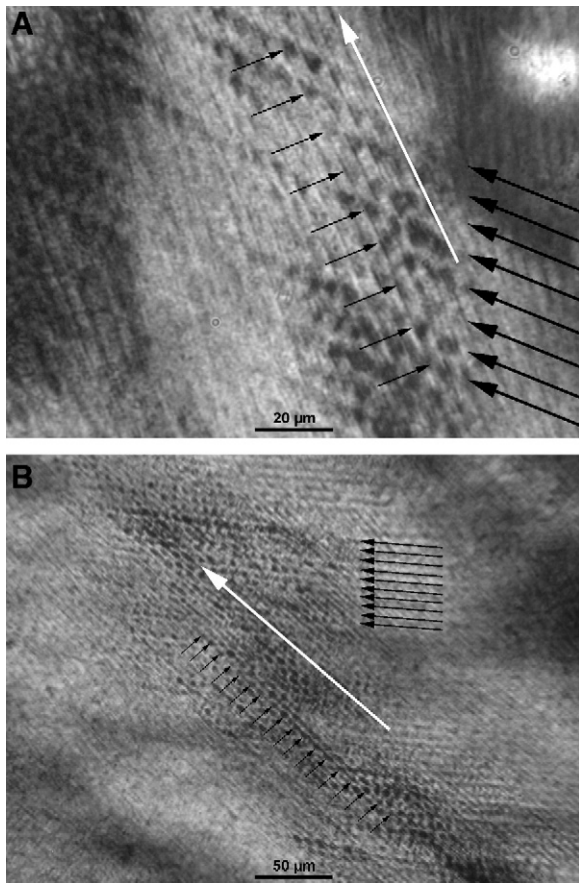


Fig. 7. Staircase shaped laminations observed on *Brachypotherium stehlini* (A) and *Diaceratherium aurelianense* (B) with two different magnifications in transmitted light microscopy. Long white arrows show directions of prisms. Long black arrows show successive laminations and short black show cross-striations along a single prism. From this it is apparent that laminations are alignments of cross-striations.

### 3.2. Large scale enamel mineralization pattern and speed of maturation

We scanned a part of the *R. unicornis* mature M<sup>1</sup> to determine the density of mature enamel among rhinoceros; this average density was  $2.46 \text{ g}_{\text{HA}}\text{cm}^{-3}$  with no significant variation from the cervix to the top of the tooth. This value is lower than the mineral density of  $2.84 \text{ g}_{\text{HA}}\text{cm}^{-3}$  for human enamel previously reported using the same protocol (Dowker et al., 2006). This difference may correspond to a higher proportion of organic matter in mature rhinoceros enamel than in human enamel, which might be related to the higher speed of dental development. We used this average density of mature rhinoceros enamel as a reference for calculations of relative mineralization of the *R.*

*sondaicus* germ, expressed both as an absolute mineral density and as the degree of relative mineralization.

The first microtomographic experiment performed with a voxel size of  $45.71 \mu\text{m}$  on a fragment of the germ of *Rhinoceros sondaicus* (Fig. 8A) failed to resolve clearly the zone of strong mineralization at the EDJ (Fig. 8B), suggesting that such a resolution too low. A second experiment performed on the same fragment and on another one with a voxel size of  $10.12 \mu\text{m}$  was used to quantify at a large scale the mineralization pattern on that germ (Fig. 8C). It revealed the highly mineralised area of enamel near the EDJ down to the cervix, but that denser thin layer appeared blurred due to limited resolution. These scans were used to determine average mineralization level of the enamel of that germ fragment, initial mineralization level of the matrix before maturation in the less mineralized areas, maximum level of mineralization observed on the largest fragment, and general maturation pattern and geometry.

According to the mineralization quantification protocol described above, we found average enamel densities respectively of  $1.33$  and  $1.12 \text{ g}_{\text{HA}}\text{cm}^{-3}$  (54.1% and 45.4% of mature enamel) for the two different fragments of the same germ shown in Fig. 8C. These values were obtained by calculating the linear absorption coefficient on 1 mm thick virtual slices in order to take into account cracks and air due to drying, assuming that they correspond to the original volume of organic matter and water. The innermost and outermost  $50 \mu\text{m}$  of enamel were not included in the calculation in order to take into account neither the highly mineralized EDJ area, nor the outer surface whose value would have been artificially lower due to border effects resulting of averaging on multiple slices.

The second germ fragment presented in Fig. 8C exhibits an outer enamel layer with several cracks. If taken into account in the density calculation, the average mineral density of that area is only  $0.67 \text{ g}_{\text{HA}}\text{cm}^{-3}$  corresponding to 27.1% of *R. unicornis* mature enamel mineral density. This area seems to have not started to mineralize, and may represent a sample very close to the initial mineral content of enamel matrix during its deposition.

That germ fragment presents a maximum mineral density of  $1.57 \text{ g}_{\text{HA}}\text{cm}^{-3}$  corresponding to 63.7% of mature enamel mineral density (Fig. 8C). Only the innermost layer of enamel near the EDJ exhibits higher mineralization level.

The two averaged enamel volumes presented in Fig. 8C (representing respectively  $11.5$  and  $9.5 \text{ mm}^3$

of enamel), give a general overview of the state of the maturation on lateral enamel at a given moment. Two main observations should be noted. First, there is no clear maturation front but a very diffuse and progressive increase of the mineral density from the

external surface towards the EDJ, in addition to the highly mineralized innermost enamel layer. Second, lines of iso-density do not correspond to the developmental pattern of the matrix. Therefore, matrix formed at different times may exhibit similar maturation

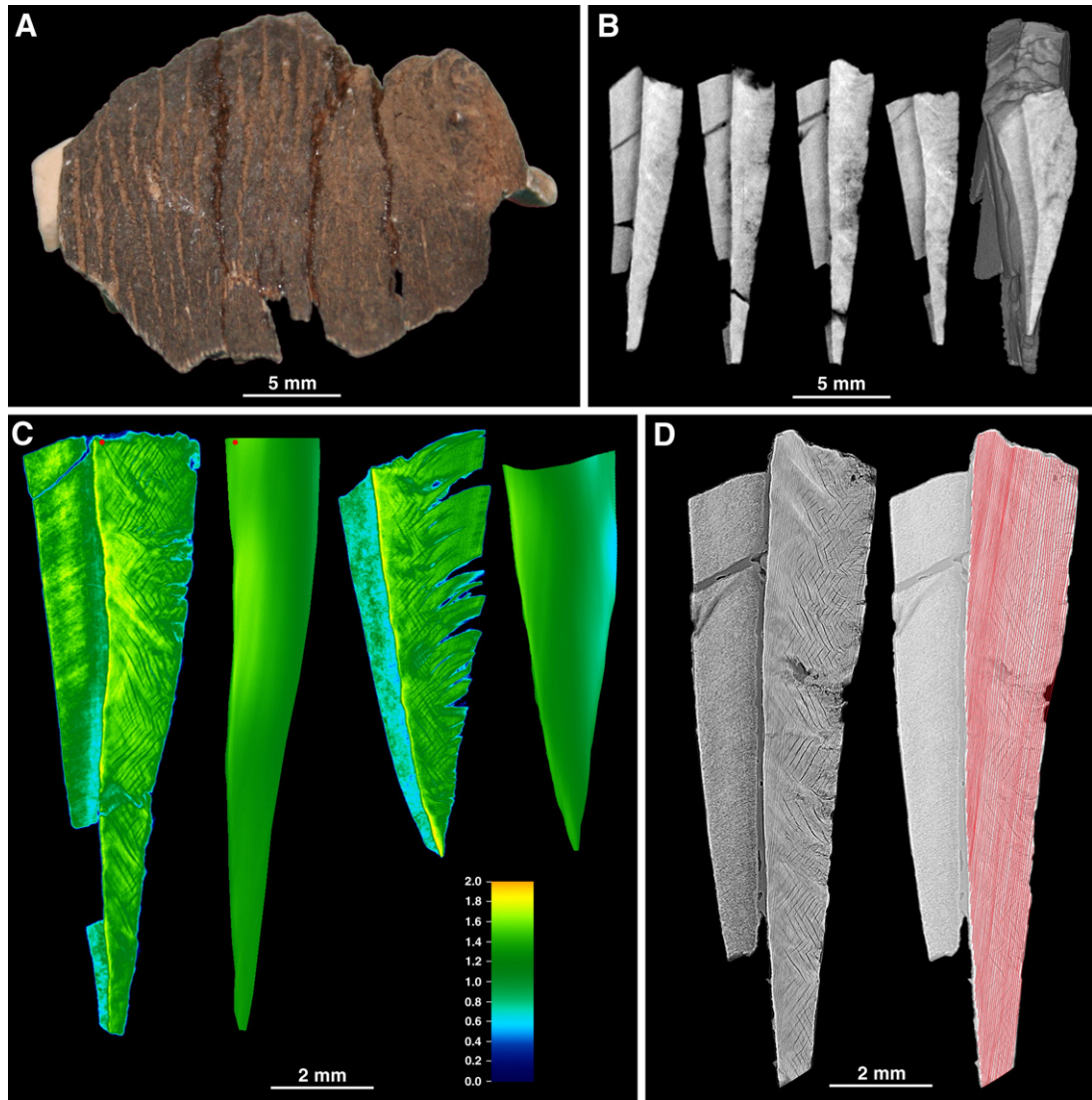


Fig. 8. X-ray synchrotron microtomographic imaging of a fragment of an early germ of a  $M^3$  of *Rhinoceros sondaicus*. A: Photograph of the germ fragment. B: Serial of virtual vertical cuts in the whole fragment generated from the scan performed in absorption mode with a voxel size of  $45.71 \mu\text{m}$ . C: Quantitative colour coding of the mineral density in  $\text{g}_{\text{HA}}\text{cm}^{-3}$  on two vertical slices in two different fragments of the germ (see text for protocol). Precise profiles are corresponding to slices with a virtual thickness of  $101.2 \mu\text{m}$  and a lateral pixel size of  $10.12 \mu\text{m}$ . Averaged slices correspond to absorption integration on a virtual slice  $1 \text{ mm}$  thick with linear averaging along EDJ and Retzius lines on  $750 \mu\text{m}$  length. This calculation allows to take into account for the average mineral density the air volume in cracks due to the desiccation and retraction of the enamel. The two red points are used for a demonstration in the text. D: Vertical slice in the principal fragment of the germ using phase contrast with a voxel size of  $5.06 \mu\text{m}$ . 10 successive slices were averaged in order to increase the relative contrast between Retzius lines and the rest of the enamel. All the Retzius lines were traced in order to estimate the developmental time recorded in that germ fragment. 67 Retzius bands were counted on that slice, representing the maximum number of Retzius lines observed on the complete fragment. On each part of the figure, dentin is on the left.

levels, and matrix formed at same time may exhibit variable maturation levels.

In order to give a temporal background to the mineralization pattern seen on the absorption scan, we performed a phase contrast scan of a part of the largest germ fragment with a  $5.06 \mu\text{m}$  isotropic voxel size. This technique revealed the Retzius lines pattern on the whole scanned volume. It showed that, despite the fact that a small part of enamel is missing at the developing cervix, the external enamel surface at the bottom of the fragment is parallel to the last Retzius line, indicating that that germ was not completed at the animal's death. We selected the best area on the scan in order to have the largest number of Retzius lines on a single slice (Fig. 8D left), and we then applied the histological Retzius lines drawing technique on the microtomographic data (Fig. 8D right). We found a total of  $67 \pm 5$  Retzius bands on that slice. Unfortunately, the high resolution scans were not performed in an area appropriate for the determination of the periodicity (showing both Retzius lines and daily incremental features). Nevertheless, as all the other rhinoceros teeth presented here exhibited a seven-day periodicity, including another third  $M^3$  of *R. sondai-cus*, we used that value to obtain a temporal estimation. The time represented on that slice was then estimated to about 469 days (1.3 years), which does not correspond to the full development time of the complete germ. Indeed, as we examined only fragments without cusp tips, this time estimation can only give a temporal baseline for the mineralization pattern on the studied fragments. More complete germs would be necessary to fully study mineralization patterns on complete teeth.

Using the general pattern of accentuated incremental lines, it was possible to register temporally all the different medium an high resolutions scans.

Combination of the tracing of Retzius lines on the phase contrast scan coupled with the density results yields can be used to estimate the maximum time between initial matrix formation on one point and full maturation of that point. For a given point situated near the top of the fragment near the EDJ but not in the innermost layer of enamel (red points on the Fig. 8C), the mineral density is about  $1.5 \text{ g}_{\text{HA}}\text{cm}^{-3}$  corresponding to 53% of *R. unicornis* mature enamel mineral density. The Retzius line number between that point and the last formed Retzius lines gives the time between the initial matrix deposition of that point and the death of the animal. Given that 67 Retzius lines are present on this germ fragment, we can consider that there are at least 60 Retzius lines

between our point and the last formed Retzius line (the slice used for absorption investigation presents slightly less Retzius bands than the one presented on Fig. 8D). These 60 bands correspond to 1.15 years assuming a seven-day periodicity. Thus, for our given point the mineralization reached only 53% of the mature enamel density 1.15 years after the initial matrix deposition.

This demonstration could be done for every point and presumably the interval between matrix deposition and full maturation would be different in different parts of the tooth. Here we are not affirming that the interval is more than 1.15 years in every area, rather it can reach more than 1.15 years in certain areas.

### 3.3. High resolution mineralization of the innermost enamel layer

A small part of the germ fragment presented in Fig. 8 was cut near the developing cervix with a wire saw for high resolution scans using absorption, phase contrast and holotomography. The size of the sample was about  $1 \text{ mm}^3$  in order to fit in the field of view of the  $1.4 \mu\text{m}$  setup. The scan in absorption was used to investigate the level of mineralization and the thickness of the innermost highly mineralized enamel with a novel degree of accuracy. Quantitative results are presented in Fig. 9A and B. Measurements of the mineral density show the mineralization pattern close to the developing cervix (about 1.5 mm from the lowest part of the image). The average mineral density of the EDJ area is  $2.06 \text{ g}_{\text{HA}}\text{cm}^{-3}$  (83.7% of the mineralization of mature enamel) for a range between 1.9 and  $2.2 \text{ g}_{\text{HA}}\text{cm}^{-3}$  (77.5–89.6% of mature enamel).

Linear measurements taken perpendicularly to the EDJ plane at different positions on that absorption scan showed that the thickness of that highly mineralized zone is relatively constant and is about  $20 \mu\text{m}$  (Fig. 9B). Fig. 9C presents an enlarged 3D block on the EDJ area, where each face of the block corresponds to an averaging of ten consecutive slices of  $1.4 \mu\text{m}$  in order to obtain a more general pattern of mineralization. That 3D bloc was then used to generate a colour quantitative density map that was superimposed with the result of the holotomographic scan at  $0.28 \mu\text{m}$  showing the enamel microstructure in 3D with the corresponding density map (Fig. 9D). From this, it is clear that the highly mineralized enamel layer corresponds to the layer of aprismatic enamel adjacent to the EDJ (Suga, 1983), plus a thin zone of prismatic radial enamel between the aprismatic layer and the

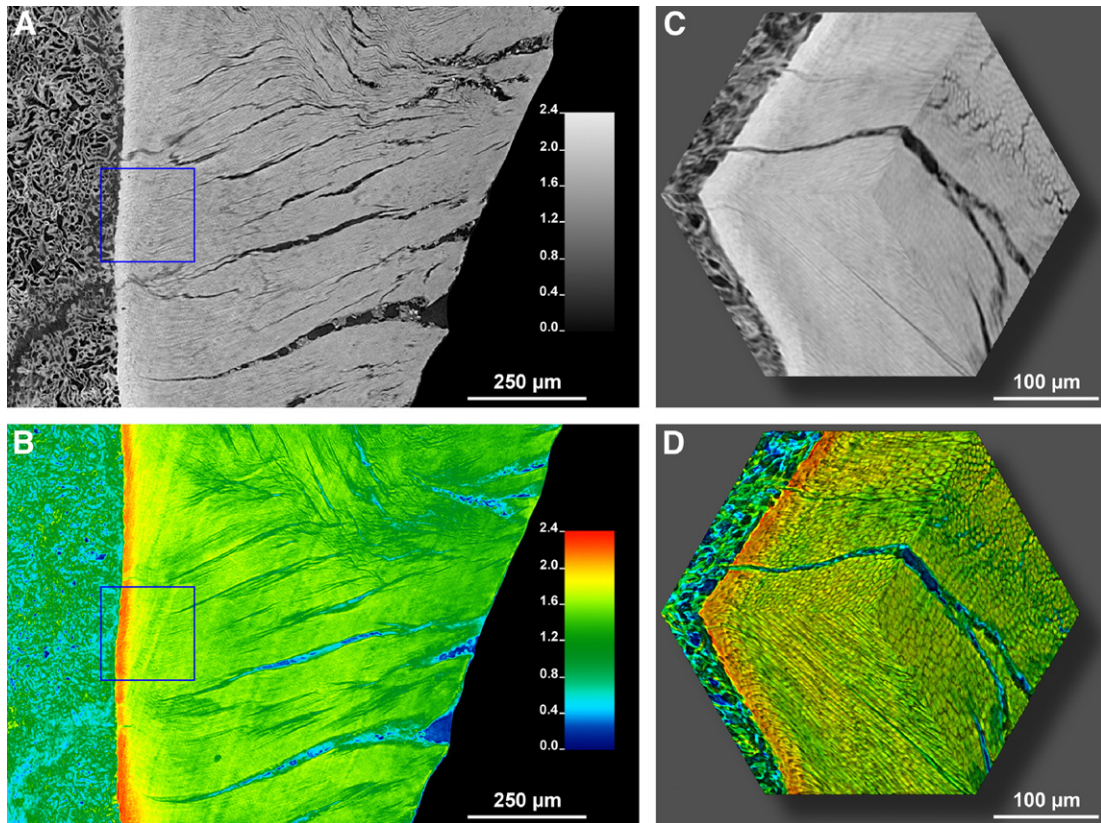


Fig. 9. High resolution microtomographic investigation of enamel mineralization and microstructure on the M<sup>3</sup> germ fragment of *Rhinoceros sondaicus*. A: Vertical slice near the cervix generated from a scan in absorption mode with an isotropic voxel size of 1.4 µm showing enamel mineral density distribution. B: Averaging of 20 slices from the same scan with quantitative colour coding of the density (same coding than in Fig. 8). The innermost enamel layer shows a higher density than the rest of the enamel on about 20 µm thick. C: 3D rendering of a 200 µm side enamel cube generated from the same scan in absorption mode corresponding to the blue boxes in part A and B. Each face is an averaging of ten slices to obtain a better visibility of the mineralization pattern. D: 3D rendering of the equivalent enamel cube generated from an holotomographic reconstruction of a phase contrast high resolution scan of the same enamel fragment. The isotropic voxel size is in that case 0.28 µm. The colours superimposed to the high resolution data come from part C of the present figure and were generated according to the quantitative colour scale presented in part B. This preparation allows to investigate the enamel microstructure linked to the highly mineralized innermost enamel layer. The cube was extracted at the limit between two Hunter-Schreger bands in order to show the prism decussations under different orientations. On each part of the figure, dentin is on the left.

prismatic enamel with strong vertical Hunter-Schreger bands typical of rhinoceros (Rensberger and Koenigswald, 1980; Boyde and Fortelius, 1986; Koenigswald, 1997).

#### 3.4. Effect of slice thickness on the visibility of daily incremental features

By using the technique of successive slices averaging presented above, we investigated the effect of the slice thickness on the predominant aspect of daily features. A small sub-volume of the holotomographic high resolution dataset was reoriented in 3D in order to be approximately perpendicular to the

Retzius plane direction (on 3D data, Retzius lines correspond to successive planes). On the slices of the new volume, Retzius lines and other incremental features remain at a nearly constant location on all the slices, while prisms or cracks are not always at the same place. Using this dataset, we generated slices with increasing thickness from 0.28 µm to 168 µm representing respectively 1 and 600 successive slices (Fig. 10).

On thin slices (from 0.28 µm to 11.2 µm) the dominant pattern of daily features is cross-striations. Nevertheless, even with a thickness of 2.8 µm, laminations become visible in the innermost enamel layer due to its nearly aprismatic structure. On the thickest slice

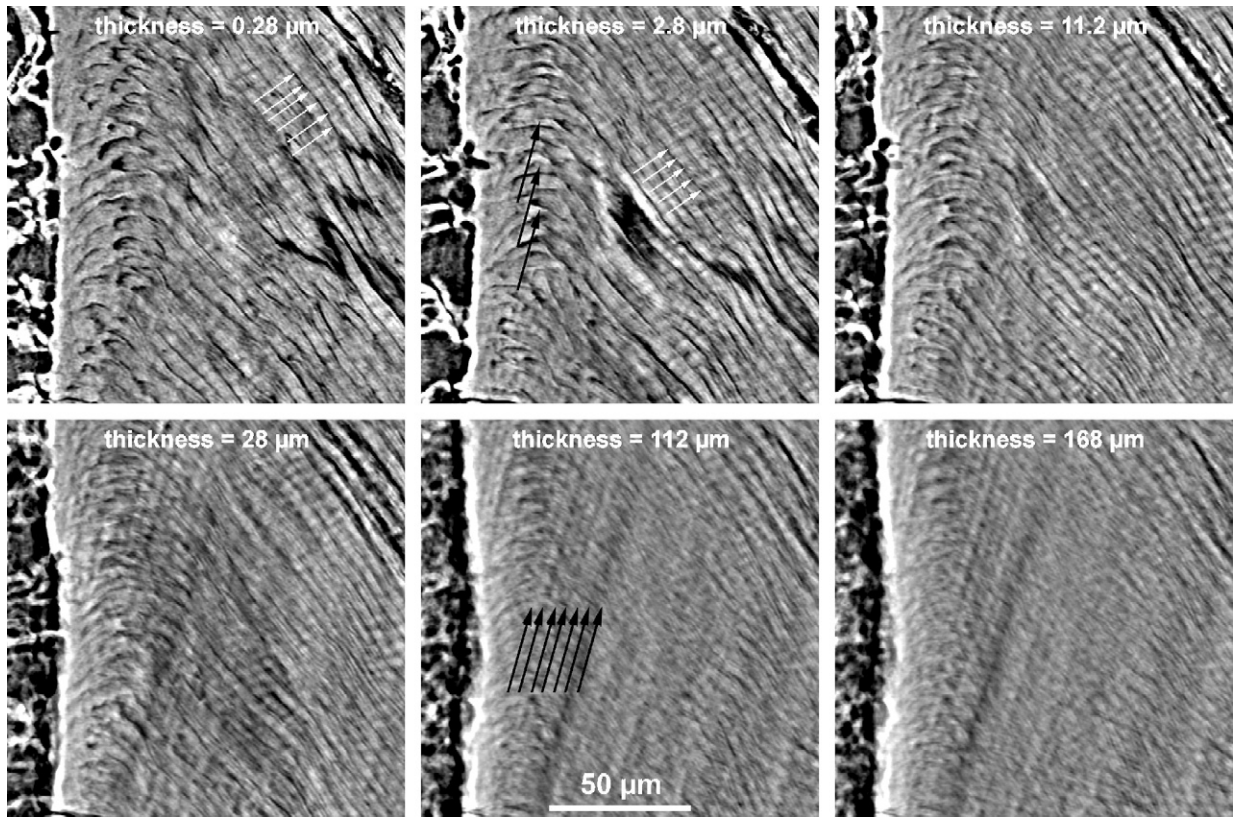


Fig. 10. Effect of the slice thickness on the visibility of fine incremental daily features. Virtual slices were generated from the holotomographic high resolution scan with a lateral pixel size of  $0.28\ \mu\text{m}$ . The thickness was increased by averaging several successive slices after a precise reorientation of the volume in the direction of the incremental features. This figure shows a progressive transition from cross-striations (white arrows) to laminations (black arrows). Dentin is on the left.

the dominant features are laminations, with spacing similar to cross-striations seen on the thin slices. Therefore increasing slice thickness shows a progressive transition from cross-striations to laminations.

#### 4. Discussion

##### 4.1. Nature of laminations

The observed laminations are apparently a daily feature in rhinoceros teeth, but despite the recent work on laminations in macaque enamel that demonstrated also a daily nature (Smith, 2004, 2006), the question of whether these features are structurally equivalent to the cross-striations described for primates and some other groups remains unresolved. Observations on rhinoceros enamel in which laminations can easily be seen, help to clarify the nature of these incremental lines in primate and other mammal teeth and to understand their relationship with cross-striations. In the following discussion, we show that these two kinds of features

are structurally equivalent and that their different frequencies in primates and rhinoceros can be explained by three different parameters acting in synergy: the slice thickness effect, the general angle between prisms and developing front, and finally the daily secretion rate.

The thickness effect can be easily explained by the fact that cross-striations are organised in 3D planes, each of these planes corresponding to a lamination parallel to the Retzius planes. Thus the thickness effect on the visibility of daily features confirms the structural equivalence between cross-striations and laminations, cross-striation effect being linked to the prismatic structure, that explains why daily incremental lines in enamel of ectothermal vertebrates appears as straight lines (Line, 2000).

The thickness effect also exists for light microscopy of histological sections, and could partially explain the difference appearances of daily features in human and rhinoceros enamel. For technical reasons it is very difficult to prepare histological sections of whole rhinoceros molars with the same thickness as human

sections (due to differential tensions between enamel and dentin, thin slides crack or unglue easily). Moreover rhinoceros enamel is characterized by very marked Hunter-Scheeger bands relative to human enamel. Therefore, physical sections of rhinoceros will be thicker with more complex enamel microstructure than human enamel, leading to greater visibility of laminations relative to cross-striations.

The second factor affecting the visibility of daily features is the angle between prisms and developing enamel front. Observation on a human molar histological slice shows laminations and cross-striations in close proximity with comparable size and pattern (Fig. 11). The only difference between these two areas is the angle between prisms and the developing enamel front, showing that it can be of relative importance on the incremental features visibility.

The third parameter influencing the visibility of daily features is the daily secretion rate. Laminations in primates enamel are generally observed near the EDJ where the prismatic structure is less developed, and in the outer part of the enamel, where the distance between successive cross-striations is maximal. In primate teeth, the spacing between cross-striations is roughly comparable to the prism diameter, which leads to a visual effect masking laminations and causing cross-striations to be the predominant pattern. Although laminations are still visible as alignments of cross-striations, they are less easily discernable due to their staircase aspect. In addition to this effect, the low enamel deposit rate in primates leads to partial overlapping between consec-

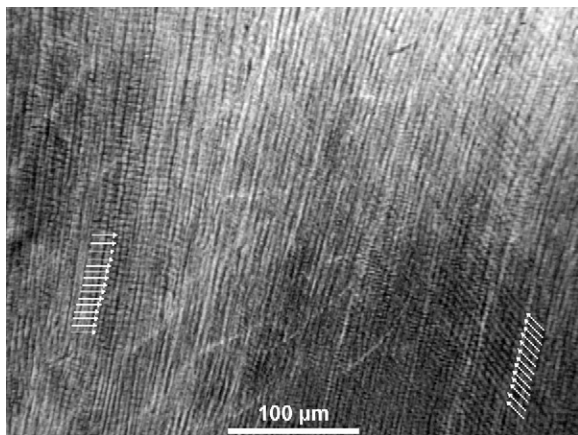


Fig. 11. Human M<sup>3</sup> observed in transmitted light microscopy. This picture presents the relationship between cross-striations (arrows on the left) and laminations (arrows on the right) and illustrates the effect of the angle between prisms and the developing enamel front on the visibility of fine incremental features.

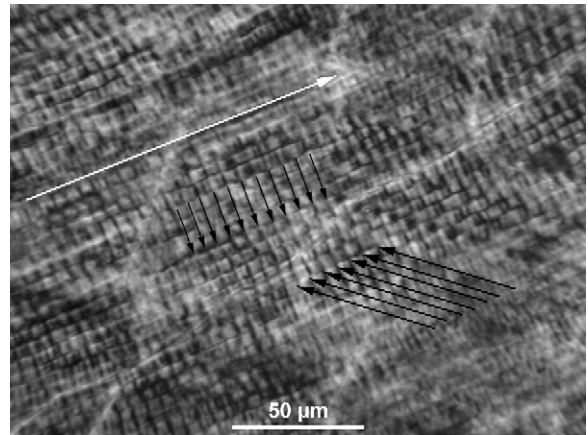


Fig. 12. Cross-striations on a human upper incisor. Despite the fact that the most evident structures are cross-striations (short black arrows), laminations are still present as alignments of these cross-striations (long black arrows). Some laminations are poorly visible due to the short distance between consecutive cross-striations that tends to mask them. White arrow shows the prism direction.

utive laminations tending to mask one out of two laminations (Fig. 12).

The Rhinoceros enamel deposition rate is higher than that of primates, and the spacing of cross-striations is larger than the diameter of prisms, which increases the visibility of the laminations. In fact, the wider the spacing of cross-striations (i.e. the enamel deposit rate), the more visible the laminations are. Fig. 13 shows a simple geometric model of this optical phenomenon for human and rhinoceros enamel. This model suggests that variations of the deposition rate can also play an important role in the observation of laminations instead of cross-striations. It clarifies also the fact that laminations in primate tooth enamel are generally observed on the outer enamel where the cross-striations are more widely spaced (Beynon et al., 1991; Dean, 1998; Smith et al., 2004).

We showed that periodicity calculated on the basis of laminations per Retzius band for rhinoceros is constant during the total formation time of the enamel: seven for at least three individual of different species of fossil and extant rhinoceros. Moreover, the fact that the estimated CFT of the different examined rhinoceros teeth are congruent with biological data for teeth formation and gestation length supports the interpretation that the laminations are daily growth features.

By the demonstration of the effect of section thickness, high-resolution holotomographic microtomography shows that laminations are due to 3D arrangements of cross-striations. This thickness effect could explain the fact that generally no laminations are

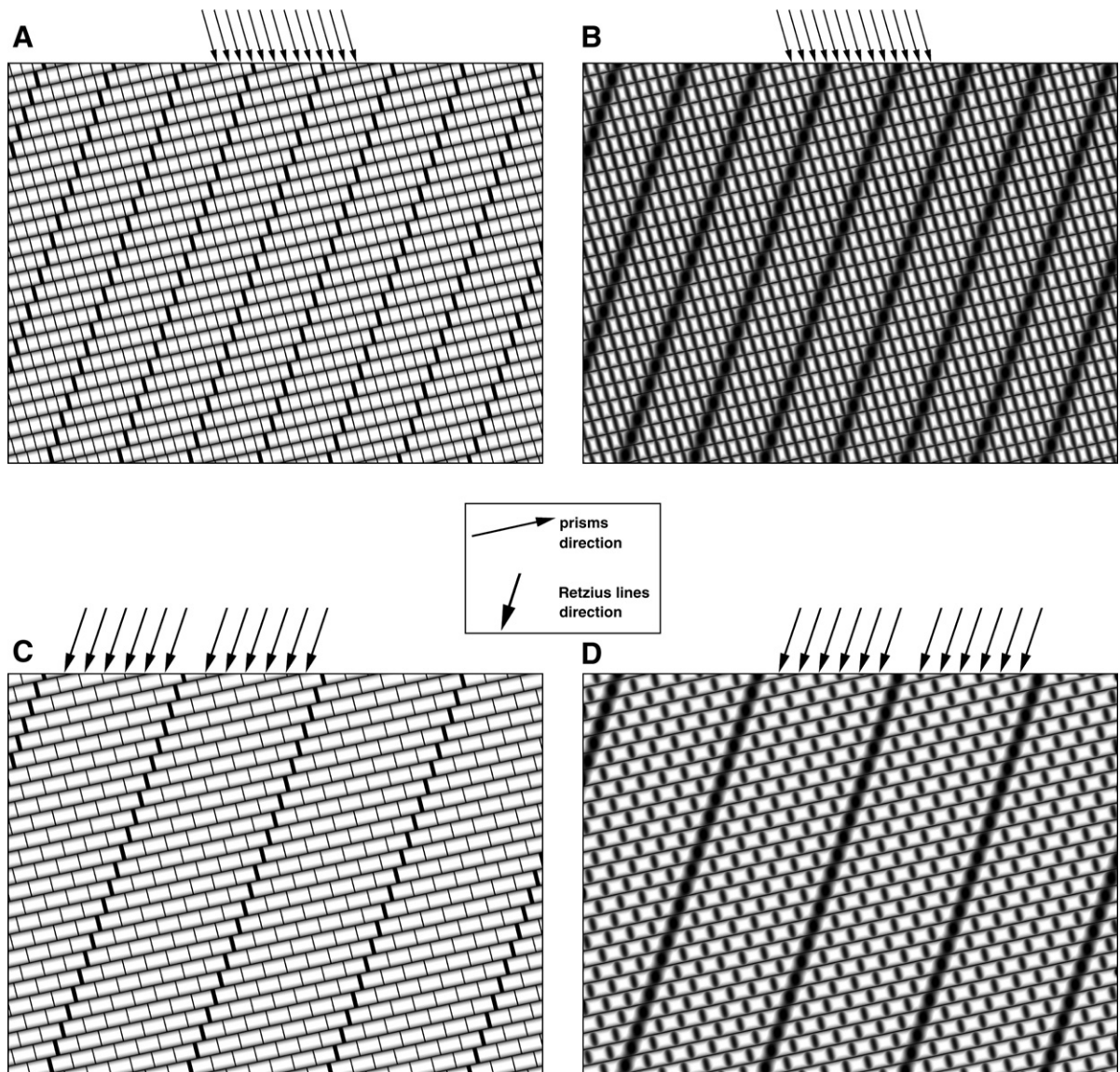


Fig. 13. Simplified geometrical model of the cross-striations / laminations phenomenon. A: model of human radial enamel with enamel deposition rate equal to prism diameter. B: same picture after the application of a Gaussian blur filter in order to obtain an image more in accordance with transmitted light microscopic enamel observations. C: model of rhinoceros radial enamel with deposit rate equal to twice the prism diameter. D: blurred picture. The serial arrows indicate the most evident kind of daily marks. The only difference between these two models is the enamel deposit rate. In B the dominant structures are cross-striations, in D the laminations are dominant.

visible with scanning electron microscopy of prismatic enamel, as the resulting micrographs only represent the surface or adjacent sub-surface structures. In some microscopic sections, laminations appear to be staircase shaped (Fig. 7), like Retzius lines in primate enamel that are formed by aligned marked cross-striations (Gustavson and Gustavson, 1967; Risnes, 1990).

In summary, we propose that laminations are daily incremental features representing a synchronic 3D front

of discrete cross-striations due to the prismatic nature of mammal enamel, which fully justifies the use of laminations for calculating time recorded in fast-forming rhinoceros enamel.

Our model of the effect of the daily secretion rate on the visibility of fine incremental marks suggests that in the majority of middle-sized and large herbivorous mammals, which have quite large teeth implying high enamel deposit rates, laminations should be the dominant pattern instead of cross-striations. Observations

on horses (Hoppe et al., 2004b), on a modern cow and a fossil *Elephantidae* (this study) confirm the presence of laminations in the enamel of these mammals (Fig. 14). Recently, a study by fluorescent marking on molars of Sika Deer (*Cervus nippon*) (Inuma et al., 2004) showed daily incremental lines in the enamel that appear to be equivalent to those observed in teeth of rhinoceros and other mammals. This additional support of our interpretation of laminations suggest that our explanation of the daily incremental marks in enamel may be generalized to several mammal groups, or perhaps even to all the mammals exhibiting incremental marks in their enamel.

Using laminations to calculate CFT for large teeth should be as precise as using cross-striations for primates teeth. Then, it would be possible to give a temporal canvas to geochemical paleoenvironmental studies if taking into account the enamel mineralization pattern in the same time.

#### 4.2. Mineralization of the enamel–dentin junction and potential implications for geochemical studies

Here we present a method to estimate the crown formation time for fossil teeth of some herbivorous mammals by using laminations and Retzius lines. However, as noted above, this calculation only gives the formation time of the enamel matrix. It does not bring the temporal pieces of information necessary to calibrate isotopic measurements on enamel performed by classical methods. Based on the microtomographic results obtained on the molar germ fragment of *Rhinoceros sondaicus*, we have demonstrated that the delay between the formation of the enamel matrix at a given point and its full maturation may exceed 1.15 years in certain areas. According to our histological and microtomographic studies, and to previous isotopic studies (Passey and Cerling, 2002; Higgins and MacFadden, 2004; Hoppe et al., 2004a,b), it seems impossible to obtain real high-resolution isotopic

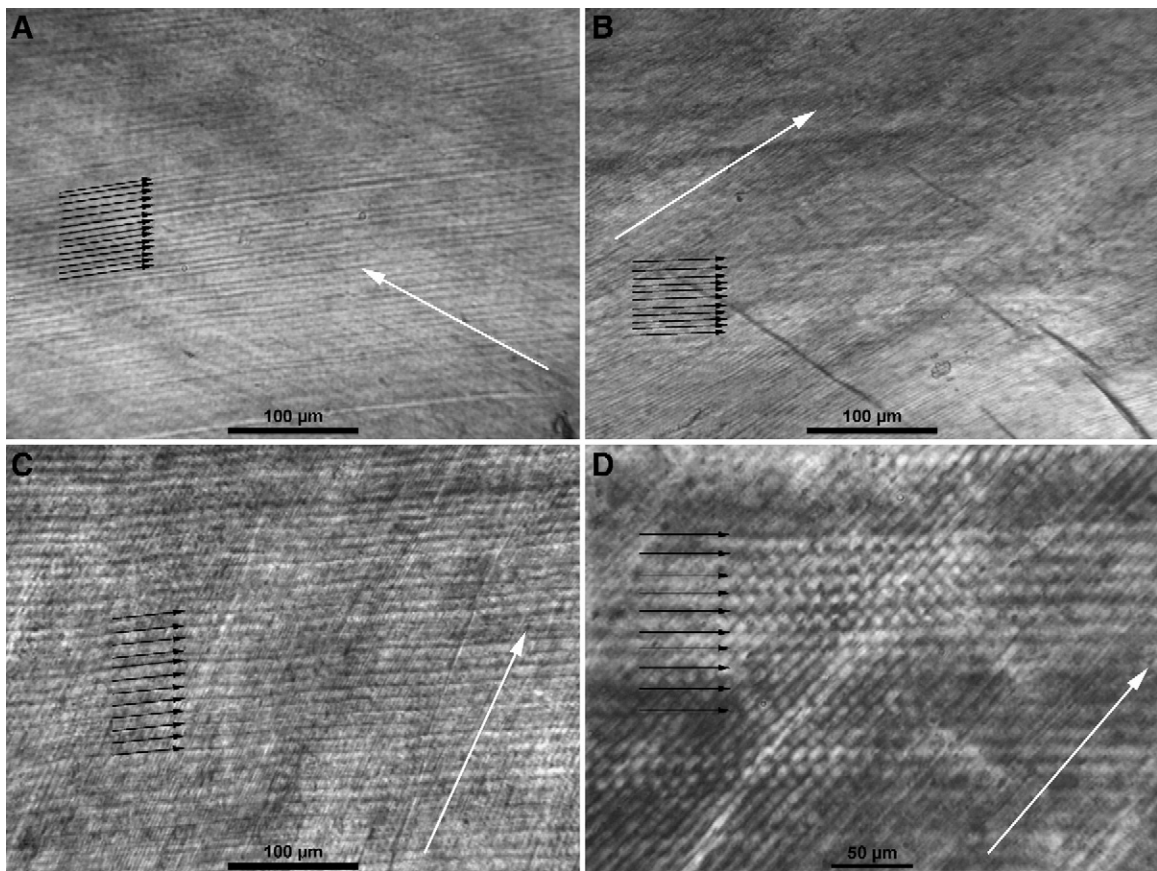


Fig. 14. Observation of laminations in some large herbivorous mammals. A: cow, B: horse, C and D: undetermined fossil *Elephantidae* from the middle Miocene site of Sansan (Gers, France). D shows that laminations are staircase shaped in this *Elephantidae*. The long white arrows show the directions of the prisms and the black ones show laminations.

records from mammalian tooth enamel due to the time averaging linked to the maturation process.

A mathematical method was proposed to reconstruct the original input signal (or something close to it) from a measured signal degraded by the maturation process (Passey and Cerling, 2002; Passey et al., 2005) by estimating several developmental parameters. This method seems to be powerful on modern samples, but it relies hypotheses that are extremely difficult or even impossible to test for fossil teeth. In particular, there is no way to know the speed of the maturation front displacement, nor its shape or the rapidity of the mineralization increase for a given point. This technique needs a well-constrained system, and cannot be substituted for real high resolution sampling when it is impossible to have all the biological and developmental data of the studied specimen, which is the case for fossil specimens.

The only remaining possibility is to perform measurements on the zone of rapid and high mineralization of the EDJ, as previously suggested (Balasse, 2003), and recently investigated by isotopic measurements (Zazzo et al., 2005). Nevertheless, the former study was performed with a too low sampling resolution to really test the value of measurements on the innermost enamel layer. According to our results, the mineralization of the enamel at the EDJ appears to be the most closely timed with the formation of incremental features, and may be able to retain about 80% of the original isotopic signal regarding to its initial mineralization level.

A limitation to isotopic analyses of this zone is its extremely small thickness (about 20  $\mu\text{m}$  in rhinoceros), which is consistent with what was observed in other mammals (Suga, 1983, 1989; Balasse, 2003; Zazzo et al., 2005). High temporal resolution isotopic investigations of enamel imply that high spatial resolution geochemical measurements have to be performed in order to sample a single point in time. Despite previous assessments (Cerling and Sharp, 1996; Sharp and Cerling, 1996; Balasse, 2003), laser ablation is not precise enough to obtain the required resolution (Zazzo et al., 2005). Micromilling can bring a better spatial precision that gives more accurate results on the EDJ (Zazzo et al., 2005), but it is still not precise enough to represent only the EDJ direct mineralization zone. Secondary Ion Mass Spectrometry (SIMS) appears to be the best potential technique, as it allows isotopic analysis on micrometric spots (Thellier et al., 2001; Tafforeau et al., 2002; Pisapia et al., 2003; Rollion-Bard et al., 2003). By combining SIMS measurements performed on the EDJ direct mineralization zone and

histological observations of the incremental marks on the same slice, it should be possible to obtain high-precision palaeoenvironmental data calibrated with the developmental time of the organism.

## 5. Conclusions

This quantitative and qualitative histological study on rhinoceros enamel demonstrated that observed laminations are temporally equivalent to cross-striations as in primate enamel. Laminations are daily markers that can be used to calculate the crown formation time of teeth of rhinoceros and potentially of the majority of middle and large sized herbivorous mammals that are characterized by high enamel secretion rates.

By using X-ray synchrotron high resolution holotomography, this study also clarified the structural status of laminations. Cross-striations and laminations correspond to different aspects of a single kind of incremental feature: the predominant appearance on slices being closely linked to the slice thickness, to the enamel deposition rate and to the angle between prisms and developing enamel front.

Laminations represent daily isochrones of the enamel deposit corresponding to serial plans of 3D alignments of cross-striations in prismatic enamel. Hence, it appears more logical to consider them as the reference daily incremental marks in enamel, with the cross-striation phenomenon being a particular aspect of laminations due to the prismatic structure of the mammalian enamel. In the case of a low deposition rate, the visual effect due to the staircase aspect of laminations hides laminations in contrast to the cross-striations, explaining the great number of observations in primate enamel, and making laminations unsuitable for calculation of CFT in this group or in any other group where the predominant incremental pattern is made of cross-striations.

Middle and high resolution X-ray synchrotron microtomographic study of an early germ of rhinoceros demonstrated a thin zone of quasi-complete mineralization linked to the EDJ. In this area the isotopic record may be almost synchronic with the matrix deposit, represented by the formation of the incremental features. Combining results on laminations and EDJ mineralization could provide a new tool for temporally registering isotopic data in the enamel of large and middle size fossil herbivorous mammals. It may minimize the effects of time averaging due to maturation in isotopic measurements used for high temporal resolution palaeoenvironmental studies. Additional studies, particularly on more complete germs at different stages of development, are required for more

accurate assessment on the potential effects of enamel maturation in isotopic records.

## Acknowledgments

We are very grateful to all the members of the ID17 and ID19 beamlines staffs at the ESRF for their precious help during the different microtomographic experiments. We would like to thank Dr. J.-A. Remy and Mr. C. Gagnaison who gave us fossil rhinoceros teeth fragments from France. We thank Dr. J. Fraga and Mrs. C. Labry (département d'imagerie Tomodoc, Clinique du millénaire, Montpellier, France) for the medical scanner images and N. Lautredou-Audouy (Centre Régional d'Imagerie Cellulaire/IURC, Montpellier, France) for the confocal microscopy. We are very grateful to C. Falguières for U/Th dating. We especially acknowledge Prof. F. Peyrin for her help in the quantitative analysis of enamel densities on microtomographic data. We are grateful to, Mr. E. Wessberge, Mrs. C. Bourigault, Dr. D. Kroon, Mr. R. Kaandorp, Dr. F. Estève and Prof. L. B. Martin for their constructive comments and corrections on previous versions. We especially acknowledge Dr. T. Smith for her invaluable help through long discussions and corrections of the paper, and for her participation to provide comparisons with primates. Finally we thanks our two anonymous reviewers since they greatly contributed to the quality of that paper through their remarks and corrections.

## References

- Allan, J.H., 1967. Maturation of enamel. In: Miles, A.E.W. (Ed.), *Structural and Chemical Organization of Teeth*. Academic Press, New York, pp. 467–494.
- Ayliffe, L.K., Lister, A.M., Chivas, A.R., 1992. The preservation of glacial–interglacial climatic signatures in the oxygen isotopes of elephant skeletal phosphate. *Palaeogeogr. Palaeoclimatol. Palaeoecol.* 99, 179–191.
- Balasse, M., 2003. Potential biases in sampling design and interpretation of intra-tooth isotope analysis. *Int. J. Osteoarcheol.* 13, 3–10.
- Balasse, M., Ambrose, S.H., Smith, A.B., Price, T.D., 2002. The seasonal mobility model for Prehistoric herders in the south-western cape of south Africa assessed by isotopic analysis of sheep tooth enamel. *J. Archaeol. Sci.* 29, 917–932.
- Baruchel, J., Cloetens, P., Hartwig, J., Ludwig, W., Mancini, L., Pernot, P., Schlenker, M., 2000. Phase contrast imaging using highly coherent X-rays: radiography, tomography, diffraction topography. *J. Synchrotron Radiat.* 7, 196–201 (Part 3).
- Baruchel, J., Lodini, A., Romanzetti, S., Rustichelli, F., Scriverani, A., 2001. Phase-contrast imaging of thin biomaterials. *Biomaterials* 22, 1515–1520.
- Benammi, M., Urrutia-Fucugauchin, J., Alva-Valdivia, L., Chaimanee, Y., Triamwihanon, S., Jaeger, J.-J., 2002. Magnetostratigraphy of the Middle Miocene continental sedimentary sequences of the Mae Moh Basin in northern Thailand: evidence for counterclockwise block rotation. *Earth Planet. Sci. Lett.* 204, 373–383.
- Beynon, A.D., Clayton, C.B., Ramirez-Rozzi, F.V., Reid, D.J., 1998. Radiographic and histological methodologies in estimating the chronology of crown development in modern humans and great apes: a review with some applications for studies on juvenile hominids. *J. Hum. Evol.* 35, 351–370.
- Beynon, A.D., Dean, M.C., Reid, D.J., 1991. On thick and thin enamel in hominoids. *Am. J. Phys. Anthropol.* 86, 295–309.
- Boyde, A., Fortelius, M., 1986. Development, structure and function of rhinoceros enamel. *Zool. J. Linn. Soc.* 87, 181–214.
- Boyde, A., Fortelius, M., Lester, K.S., Martin, L.B., 1988. Basis of the structure and development of mammalian enamel as seen by scanning electron microscopy. *Scan. Microsc.* 2 (3), 1479–1490.
- Bromage, T.G., 1991. Enamel incremental periodicity in the pig-tailed macaque: a polychrome fluorescent labeling study of dental hard tissues. *Am. J. Phys. Anthropol.* 86, 205–214.
- Bryant, J.D., Luz, B., Froelich, P.N., 1994. Oxygen isotopic composition of fossil horse tooth phosphate as a record of continental paleoclimate. *Palaeogeogr. Palaeoclimatol. Palaeoecol.* 107, 303–316.
- Bryant, J.D., Froelich, P.N., Showers, W.J., Genna, B.J., 1996. A tale of two quarries: biologic and taphonomic signatures in the oxygen isotope composition of tooth enamel phosphate from modern and miocene equids. *Palaios* 11, 397–408.
- Buffière, J.Y., Maire, E., Cloetens, P., Lormand, G., Fougères, R., 1999. Characterization of internal damage in a MMCp using x-ray synchrotron phase contrast microtomography. *Acta Mater.* 47 (5), 1613–1625.
- Cerling, T.E., Sharp, Z.D., 1996. Stable carbon and oxygen isotope analysis of fossil enamel using laser ablation. *Palaeogeogr. Palaeoclimatol. Palaeoecol.* 126, 173–186.
- Chaimanee, Y., Jolly, D., Benammi, M., Tafforeau, P., Duzer, D., Moussa, I., Jaeger, J.-J., 2003. A Middle Miocene hominoid from Thailand and orangutan origins. *Nature* 422, 61–65.
- Cloetens, P., Baruchel, J., Van Dyck, D., Van Landuyt, J., Guigay, J.-P., Schlenker, M., 1999a. Holotomography: quantitative phase tomography with micrometer resolution using hard synchrotron radiation X-rays. *Appl. Phys. Lett.* 75 (19), 2912–2914.
- Cloetens, P., Ludwig, W., Baruchel, J., Guigay, J.-P., Perno-Rejmankova, P., Salome-Pateyron, M., Schlenker, M., Buffiere, J.-Y., Maire, E., Peix, G., 1999b. Hard X-ray phase imaging using simple propagation of a coherent synchrotron radiation beam. *J. Appl. Phys.* 32, A145–A151 (10A Sp. Iss.).
- Dean, M.C., 1987. Growth layers and incremental markings in hard tissues; a review of the literature and some preliminary observations about enamel structure in *Paranthropus boisei*. *J. Hum. Evol.* 16, 157–172.
- Dean, M.C., 1998. A comparative study of cross striation spacing in cuspal enamel and of four methods of estimating the time taken to grow molar cuspal enamel in *Pan*, *Pongo* and *Homo*. *J. Hum. Evol.* 35, 449–462.
- Dean, M.C., Schrenk, F., 2003. Enamel thickness and development in a third permanent molar of *Gigantopithecus blacki*. *J. Hum. Evol.* 45, 381–387.
- Dean, M.C., Beynon, A.D., Thackeray, J.F., Macho, G.A., 1993. Histological reconstruction of dental development and age at death of a juvenile *Paranthropus robustus* specimen, SK 63, from Swartkrans, South Africa. *Am. J. Phys. Anthropol.* 91, 401–419.
- Dirks, W., Reid, D.J., Jolly, C.J., Phillips-Conroy, J.E., Brett, F.L., 2002. Out of the mouth of baboons: stress, life history, and dental

- development in the Awash National Park Hybrid Zone, Ethiopia. *Am. J. Phys. Anthropol.* 118, 239–252.
- Dowker, S.E.P., Elliott, J.C., Davis, R.M., Wilson, R.M., Cloetens, P., 2004. Synchrotron X-ray microtomographic investigation of mineral concentrations at micrometer scale in sound and carious enamel. *Caries Res.* 38, 514–522.
- Dowker, S.E.P., Elliott, J.C., Davis, G.R., Wilson, R.M., Cloetens, P., 2006. Three-dimensional study of human dental fissure enamel by synchrotron X-ray microtomography. *Eur. J. Oral Sci.* 114 (suppl. 1), 353–359.
- Ducrocq, S., Chaimanee, Y., Suteethorn, V., Jaeger, J.-J., 1995. Mammalian faunas and the ages of the continental Tertiary fossiliferous localities from Thailand. *J. Southeast Asian Earth Sci.* 12 (1/2), 65–78.
- Fearnhead, R.W., 1984. Preface. In: Fearnhead, R.W., Suga, S. (Eds.), *Tooth Enamel IV*. Elsevier Science Publishers B. V., Amsterdam, pp. V–VI.
- Feist, M., Liu, J., Tafforeau, P., 2005. New insights into Paleozoic charophyte morphology and phylogeny. *Am. J. Bot.* 92, 1152–1160.
- Fitzgerald, 1998. Do enamel microstructure have regular time dependency? Conclusions from the literature and a large-scale study. *J. Hum. Evol.* 35, 371–386.
- Fox, D.L., Fisher, D.C., 2001. Stable isotope ecology of a Late Miocene population of *Gomphotherium productus* (Mammalia, Proboscidea) from Port of Entry Pit, Oklahoma, USA. *Palaios* 16, 279–293.
- Gadbury, C., Todd, L., Jähren, A.H., Amundson, R., 2000. Spatial and temporal variations in the isotopic composition of bison tooth enamel from the early Holocene Hudson-meng Bone Bed, Nebraska. *Palaeogeogr. Palaeoclimatol. Palaeoecol.* 157, 79–93.
- Gustavson, G., Gustavson, A.-G., 1967. Microanatomy and Histochemistry of enamel. In: Miles, A.E.W. (Ed.), *Structural and Chemical Organization of Teeth*. Academic press, New York, pp. 75–134.
- Higgins, P., MacFadden, B.J., 2004. “Amount Effect” recorded in oxygen isotopes of Late Glacial horse (*Equus*) and bison (*Bison*) teeth from the Sonoran and Chihuahuan deserts, southwestern United States. *Palaeogeogr. Palaeoclimatol. Palaeoecol.* 206, 337–353.
- Hillman-Smith, A.K.K., Owen-Smith, N., Anderson, J.L., Hall-Martin, A.J., Selaladi, J.P., 1986. Age estimation of the white rhinoceros (*Ceratotherium simum*). *J. Zool.* 210, 355–379.
- Hoppe, K.A., Amundson, R.M.V., McClaran, M.P., Anderson, D.L., 2004a. Isotopic analysis of tooth enamel carbonate from modern North American feral horses: implications for paleoenvironmental reconstructions. *Palaeogeogr. Palaeoclimatol. Palaeoecol.* 203, 299–311.
- Hoppe, K.A., Stover, S.M., Pascoe, J.R., Amundson, R., 2004b. Tooth enamel biomineralization in extant horses: implications for isotopic microsampling. *Palaeogeogr. Palaeoclimatol. Palaeoecol.* 206 (3–4), 355–365.
- Iacumin, P., Bocherens, H., Mariotti, A., Longinelli, A., 1996. Oxygen isotope analyses of co-existing carbonate and phosphate in biogenic apatite: a way to monitor diagenetic alteration of bone phosphate? *Earth Planet. Sci. Lett.* 142, 1–6.
- Iinuma, Y.M., Tanaka, S., Kawasaki, K., Kuwajima, T., Nomura, H., Suzuki, M., Ohtaishi, N., 2004. Dental incremental lines in Sika Deer (*Cervus nippon*); polarized light and fluorescence microscopy of ground sections. *J. Vet. Med. Sci.* 66 (6), 665–669.
- Kelley, J., Smith, T.M., 2003. Age at first molar emergence in early Miocene *Afropithecus turkanensis* and life-history evolution in the Hominoidea. *J. Hum. Evol.* 44, 307–329.
- Koenigswald, W.v., 1997. Brief survey of enamel diversity at the schmelzmuster level in Cenozoic placental mammals. In: Koenigswald, W.v., Sander, P.M. (Eds.), *Tooth Enamel Microstructure*. A. A. Balkema, Rotterdam, pp. 137–161.
- Line, S.R.P., 2000. Incremental markings of enamel in ectothermal vertebrates. *Arch. Oral Biol.* 45, 363–368.
- Longinelli, A., 1984. Oxygen isotopes in mammal bone phosphate: a new tool for paleohydrological and paleoclimatological research? *Geochim. Cosmochim. Acta* 48, 385–390.
- Macho, G.A., Leakey, M.G., Williamson, D.K., Jiang, Y., 2003. Paleoenvironmental reconstruction: evidence for seasonality at Allia Bay, Kenya, at 3.9 million years. *Palaeogeogr. Palaeoclimatol. Palaeoecol.* 199, 17–30.
- Moss-Salentijn, L., Moss, M.L., Sheng-Tien Yuan, M., 1997. The ontogeny of mammalian enamel. In: Koenigswald, W.v., Sander, P.M. (Eds.), *Tooth Enamel Microstructure*. A. A. Balkema, Rotterdam, pp. 5–30.
- Nuzzo, S., Peyrin, F., Cloetens, P., Baruchel, J., Boivin, G., 2002. Quantification of the degree of mineralization of bone in three dimensions using synchronisation radiation microtomography. *Med. Phys.* 29 (11), 2672–2681.
- Owen-Smith, N., 1995. Rhinoceroses. In: Macdonald, D. (Ed.), *The Encyclopedia of Mammals*. Andromeda Oxford Ltd, Oxford, pp. 490–497.
- Passay, B.H., Cerling, T.E., 2002. Tooth enamel mineralization in ungulates: implications for recovering a primary isotopic time-series. *Geochim. Cosmochim. Acta* 66 (18), 3225–3234.
- Passay, B.H., Cerling, T.E., Schuster, G.T., Robinson, T.F., Roeder, B.L., Krueger, S.K., 2005. Inverse methods for estimating primary input signals from time-averaged isotope profiles. *Geochim. Cosmochim. Acta* 69 (16), 4101–4116.
- Pisapia, C., Bentaleb, I., Rollion-Bard, C., Tafforeau, P., Fontugne, M., France-Lanord, C., 2003. High resolution measurement of  $^{18}\text{O}/^{16}\text{O}$  ratios of present and fossil herbivores dental enamel using the IMS 1270 ion microprobe. *Geophys. Res. Abstr.* 5, 03781.
- Ramirez-Rozzi, F.V., 1993. Microstructure et développement de l’émail dentaire du néandertalien de Zafarraya, Espagne. Temps de formation et hypocalcification de l’émail dentaire. *C. R. Acad. Sci. Paris Série II* 316, 1635–1642.
- Reid, D.J., Beynon, A.D., Ramirez-rozzi, F.V., 1998a. Histological reconstruction of dental development in four individuals from a medieval site in Picardie, France. *J. Hum. Evol.* 35, 463–477.
- Reid, D.J., Schwartz, G.T., Dean, C., Chandrasekera, M.S., 1998b. A histological reconstruction of dental development in the common chimpanzee, *Pan troglodytes*. *J. Hum. Evol.* 35, 427–448.
- Reith, E.J., Butcher, E.O., 1967. Microanatomy and histochemistry of amelogenesis. In: Miles, A.E. (Ed.), *Structural and Chemical Organization of Teeth*. Academic Press, New York, pp. 371–397.
- Rensberger, J.M., Koenigswald, W.v., 1980. Functional and phylogenetic interpretation of enamel microstructure in rhinoceroses. *Paleobiology* 6 (4), 477–495.
- Risnes, S., 1986. Enamel apposition rate and the prism periodicity in human teeth. *Scand. J. Dent. Res.* 94, 394–404.
- Risnes, S., 1990. Structural characteristics of staircase-type Retzius lines in human dental enamel analyzed by scanning electron microscopy. *Anat. Rec.* 226, 135–146.
- Risnes, S., 1998. Growth tracks in dental enamel. *J. Hum. Evol.* 35, 331–350.
- Rollion-Bard, C., Blamart, D., Cuif, J.P., Juillet-Leclerc, A., 2003. Microanalysis of C and O isotopes of azooxanthellate and zooxanthellate corals by ion microprobe. *Reefs* 22 (4), 405–415.
- Sakae, T., Suzuki, K., Kozawa, Y., 1997. A short review of studies on chemical and physical properties of enamel crystallites. In: Koenigswald, W.v., Sander, P.M. (Eds.), *Tooth Enamel Microstructure*. A. A. Balkema, Rotterdam, pp. 31–39.

- Salvo, L., Cloetens, P., Maire, E., Zabler, S., Blandin, J.J., Buffière, J.Y., Ludwig, W., Boller, E., Bellet, D., Josserson, C., 2003. X-ray microtomography an attractive characterisation technique in materials science. Nucl. Instrum. Methods Phys. Res., B 200, 273–286.
- Schwartz, G.T., Reid, D.J., Dean, C., 2001. Developmental aspects of sexual dimorphism in Hominoid canines. Int. J. Primatol. 22 (5), 837–860.
- Schwartz, G.T., Liu, W., Zheng, L., 2003. Preliminary investigation of dental microstructure in the Yuanmou hominoid (*Lufeng-*), Yunnan Province, China. J. Hum. Evol. 44, 189–202.
- Sharp, Z.D., Cerling, T.E., 1996. A laser GC-IRMS technique for in situ stable isotope analyses of carbonates and phosphates. Geochim. Cosmochim. Acta 60 (15), 2909–2916.
- Shellis, R.P., 1998. Utilisation of periodic markings in enamel to obtain information on tooth growth. J. Hum. Evol. 35, 387–400.
- Smith, T.M., 2004. Incremental Development of Primate Dental Enamel. PhD Thesis, Stony Brook University, Stony Brook, 370 pp.
- Smith, T.M., 2006. Experimental determination of the periodicity of incremental features in enamel. J. Anat. 208, 99–113.
- Smith, T.M., Martin, L.B., Leakey, M.G., 2003. Enamel thickness, microstructure and development in *Afropithecus turkanensis*. J. Hum. Evol. 44, 283–306.
- Smith, T.M., Martin, L.B., Reid, D.J., de Bonis, L., Koufos, G.D., 2004. An examination of dental development in *Graecopithecus freybergi* (= *Ouranopithecus macedoniensis*). J. Hum. Evol. 46 (5), 551–577.
- Suga, S., 1983. Comparative histology of the progressive mineralization pattern of developing enamel. In: Suga, S. (Ed.), Mechanisms of Tooth Enamel Formation. Quintessence Publishing, Tokyo, pp. 167–203.
- Suga, S., 1989. Enamel hypomineralization viewed from the pattern of progressive mineralization of human and monkey developing enamel. Adv. Dent. Res. 3, 188–198.
- Tafforeau, P., 2004. Aspects phylogénétiques et fonctionnels de la microstructure de l'émail dentaire et de la structure tridimensionnelle des molaires chez les primates fossiles et actuels: apports de la microtomographie à rayonnement X synchrotron. Ph.D. Thesis, Université de Montpellier II, France, 294 pp.
- Tafforeau, M., Verdus, M.-C., Norris, V., White, G., Demarty, M., Thellier, M., Ripoll, C., 2002. SIMS study of the calcium-deprivation step related to epidermal meristem production induced in flax by cold shock or radiation from a GSM telephone. J. Trace Microprobe Tech. 20 (4), 611–623.
- Tafforeau, P., Boistel, R., Boller, E., Bravin, A., Brunet, M., Chaimanee, Y., Cloetens, P., Feist, M., Horszowska, J., Jaeger, J.-J., Kay, R.F., Lazzari, V., Marivaux, L., Nel, A., Nemoz, C., Thibault, X., Vignaud, P., Zabler, S., 2006. Applications of X-ray synchrotron microtomography for non-destructive 3D studies of paleontological specimens. Appl. Phys., A Mater. Sci. Process. 83, 195–202.
- Thellier, M., Dérue, C., Tafforeau, M., Le Sceller, L., Verdus, M.-C., Massiot, P., Ripoll, C., 2001. Physical methods for in vitro analytical imaging in the microscopic range in biology, using radioactive or stable isotopes (review article). J. Trace Microprobe Tech. 19 (1), 143–162.
- Zazzo, A., Mariotti, A., Lécuyer, C., Heintz, E., 2002. Intra-tooth isotope variations in late Miocene bovid enamel from Afghanistan: paleobiological, taphonomic, and climatic implications. Palaeogeogr. Palaeoclimatol. Palaeoecol. 186, 145–161.
- Zazzo, A., Balasse, M., Patterson, W.P., 2005. High-resolution  $\delta^{13}\text{C}$  intratooth profiles in bovine enamel: implications for mineralization pattern and isotopic attenuation. Geochim. Cosmochim. Acta 69 (14), 3631–3642.